Article

Developmental Cell

The Germ Cell Fate of Cynomolgus Monkeys Is Specified in the Nascent Amnion

Graphical Abstract

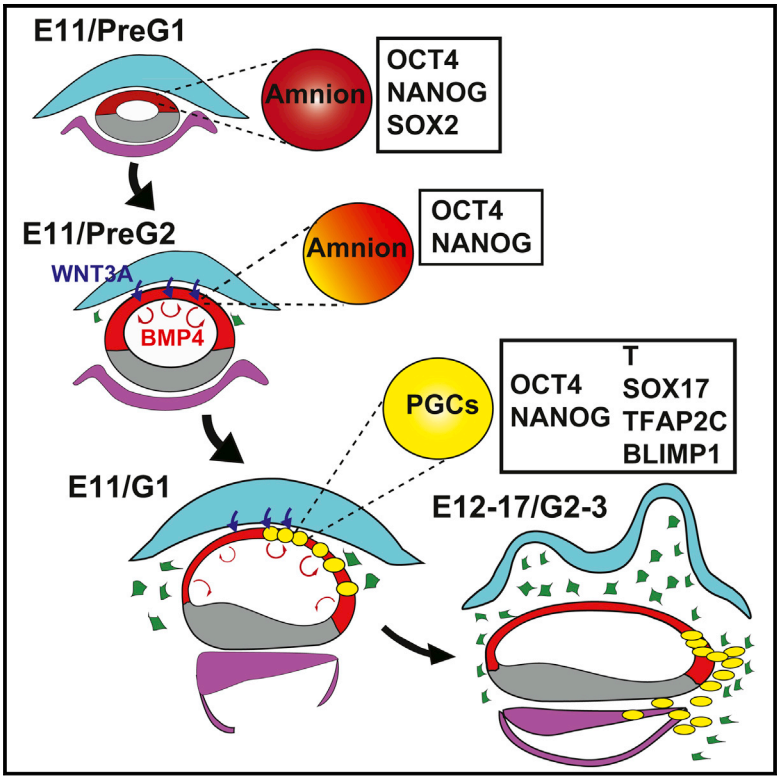

Authors

Kotaro Sasaki, Tomonori Nakamura, Ikuhiro Okamoto, ..., Tetsuya Takakuwa, Takuya Yamamoto, Mitinori Saitou

Correspondence

saitou@anat2.med.kyoto-u.ac.jp

In Brief

How primordial germ cells (PGCs) are specified in primate (including human) development is unknown. Sasaki et al. show that in cynomolgus monkeys, PGCs are specified in the early amnion, which may be an autocrine signaling center for specification. In-vitro-specified human PGCs exhibit a transcriptome similar to that of early monkey PGCs.

Highlights

- A comprehensive analysis of PGC development in cynomolgus monkeys
- cyPGCs originate in the nascent amnion prior to gastrulation of the epiblast
- The amnion itself expresses and responds to signals for PGC specification
- Human PGC-like cell transcriptome is similar to cyPGCs just after specification

Accession Numbers

GSE76267
GSE74767
GSE67259

Sasaki et al., 2016, Developmental Cell *39*, 1–17
October 24, 2016
http://dx.doi.org/10.1016/j.devcel.2016.09.007

CellPress

Please cite this article in press as: Sasaki et al., The Germ Cell Fate of Cynomolgus Monkeys Is Specified in the Nascent Amnion, Developmental Cell (2016), http://dx.doi.org/10.1016/j.devcel.2016.09.007

Developmental Cell
Article

The Germ Cell Fate of Cynomolgus Monkeys Is Specified in the Nascent Amnion

Kotaro Sasaki,[1,2] Tomonori Nakamura,[1,2] Ikuhiro Okamoto,[1,2] Yukihiro Yabuta,[1,2] Chizuru Iwatani,[2,3] Hideaki Tsuchiya,[2,3] Yasunari Seita,[2,3] Shinichiro Nakamura,[2,3] Naoto Shiraki,[4] Tetsuya Takakuwa,[4] Takuya Yamamoto,[5,6,7] and Mitinori Saitou[1,2,5,6,8,*]

[1]Department of Anatomy and Cell Biology, Graduate School of Medicine, Kyoto University, Yoshida-Konoe-cho, Sakyo-ku, Kyoto 606-8501, Japan
[2]JST, ERATO, Yoshida-Konoe-cho, Sakyo-ku, Kyoto 606-8501, Japan
[3]Research Center for Animal Life Science, Shiga University of Medical Science, Seta-Tsukinowa-cho, Otsu, Shiga 520-2192, Japan
[4]Human Health Sciences, Graduate School of Medicine, Kyoto University, Shogoin Kawahara-cho 53, Sakyo-ku, Kyoto 606-8507, Japan
[5]Center for iPS Cell Research and Application, Kyoto University, 53 Kawahara-cho, Shogoin, Sakyo-ku, Kyoto 606-8507, Japan
[6]Institute for Integrated Cell-Material Sciences, Kyoto University, Yoshida-Ushinomiya-cho, Sakyo-ku, Kyoto 606-8501, Japan
[7]AMED-CREST, AMED, 1-7-1 Otemachi, Chiyoda-ku, Tokyo 100-0004, Japan
[8]Lead Contact
*Correspondence: saitou@anat2.med.kyoto-u.ac.jp
http://dx.doi.org/10.1016/j.devcel.2016.09.007

SUMMARY

The germ cell lineage ensures reproduction and heredity. The mechanism for germ cell specification in primates, including humans, has remained unknown. In primates, upon implantation the pluripotent epiblast segregates the amnion, an extra-embryonic membrane eventually ensheathing an embryo, and thereafter initiates gastrulation to generate three germ layers. Here, we show that in cynomolgus monkeys, the SOX17/TFAP2C/BLIMP1-positive primordial germ cells (cyPGCs) originate from the dorsal amnion at embryonic day 11 (E11) prior to gastrulation. cyPGCs appear to migrate down the amnion and, through proliferation and recruitment from the posterior amnion, expand in number around the posterior yolk sac by E17. Remarkably, the amnion itself expresses BMP4 and WNT3A, cytokines potentially critical for cyPGC specification, and responds primarily to them. Moreover, human PGC-like cells in vitro exhibit a transcriptome similar to cyPGCs just after specification. Our study identifies the origin of PGCs and a unique function of the nascent amnion in primates.

INTRODUCTION

During development, specification of primordial germ cells (PGCs), the precursors both for the spermatozoa and the oocytes, heralds the creation of new organisms and is essential for the evolution and continuity of life. There exist two major mechanisms for PGC specification among metazoans: one is through inheritance of the preformed germ plasm, as originally proposed by August Weismann (Weismann, 1892), and the other is through induction by signaling molecules in pluripotent embryonic cells (Extavour and Akam, 2003). Although the former has become prevalent presumably through convergent evolution, the latter appears to be the ancestral mechanism, and it is most likely that all mammals, including humans, generate PGCs by the latter mode (Extavour and Akam, 2003).

The mechanism for mammalian germ cell specification has been studied most extensively using mice as a model organism (Saitou and Yamaji, 2012). The mouse pre-gastrulating epiblast exhibits a cylindrical shape and bears a uniform competence for the germ cell fate between embryonic day 5.5 (E5.5) and E6.25. A balanced action of inductive and restrictive signals allocates the germ cell fate in the most proximal posterior epiblast at around E6.0: inductive signals include bone morphogenetic protein 4 (BMP4) from the extra-embryonic ectoderm in direct contact with the proximal epiblast and WNT3 from the proximal posterior epiblast itself, and restrictive signals include CER1 and DKK1 from the anterior visceral endoderm (Lawson et al., 1999; Ohinata et al., 2009). Consequently, mouse PGCs (mPGCs) of approximately 30–40 in number (Ginsburg et al., 1990; Saitou et al., 2002) that express the key transcription factors (TFs) BLIMP1 (also known as PRDM1), PRDM14, and TFAP2C (also known as AP2γ), are established within the extra-embryonic mesoderm at around E7.25 (Kurimoto et al., 2008; Ohinata et al., 2005; Vincent et al., 2005; Weber et al., 2010; Yamaji et al., 2008), and undergo migration toward future gonads for spermatogenic or oogenic differentiation (McLaren, 2003).

On the other hand, mammalian early development involves substantial divergence in the mechanism and order of cell-fate allocations among species (Rossant, 2015), and there has been a critical lack of information regarding the mechanism for PGC specification in mammals other than mice. In primates, upon implantation the epiblast segregates the amnion to form the amniotic cavity and acquires a disc-like shape, and the hypoblast, while generating the visceral endoderm (VE) and parietal endoderm (PE) to form the secondary yolk sac, gives rise to the extra-embryonic mesenchyme, which occupies the space between the cytotrophoblast and the amnion (Enders, 2007; Enders and King, 1988; Enders et al., 1986; Heuser and Streeter, 1941; Luckett, 1978; Nakamura et al., 2016). Thus, the anatomical structure of primate embryos at stages relevant for PGC

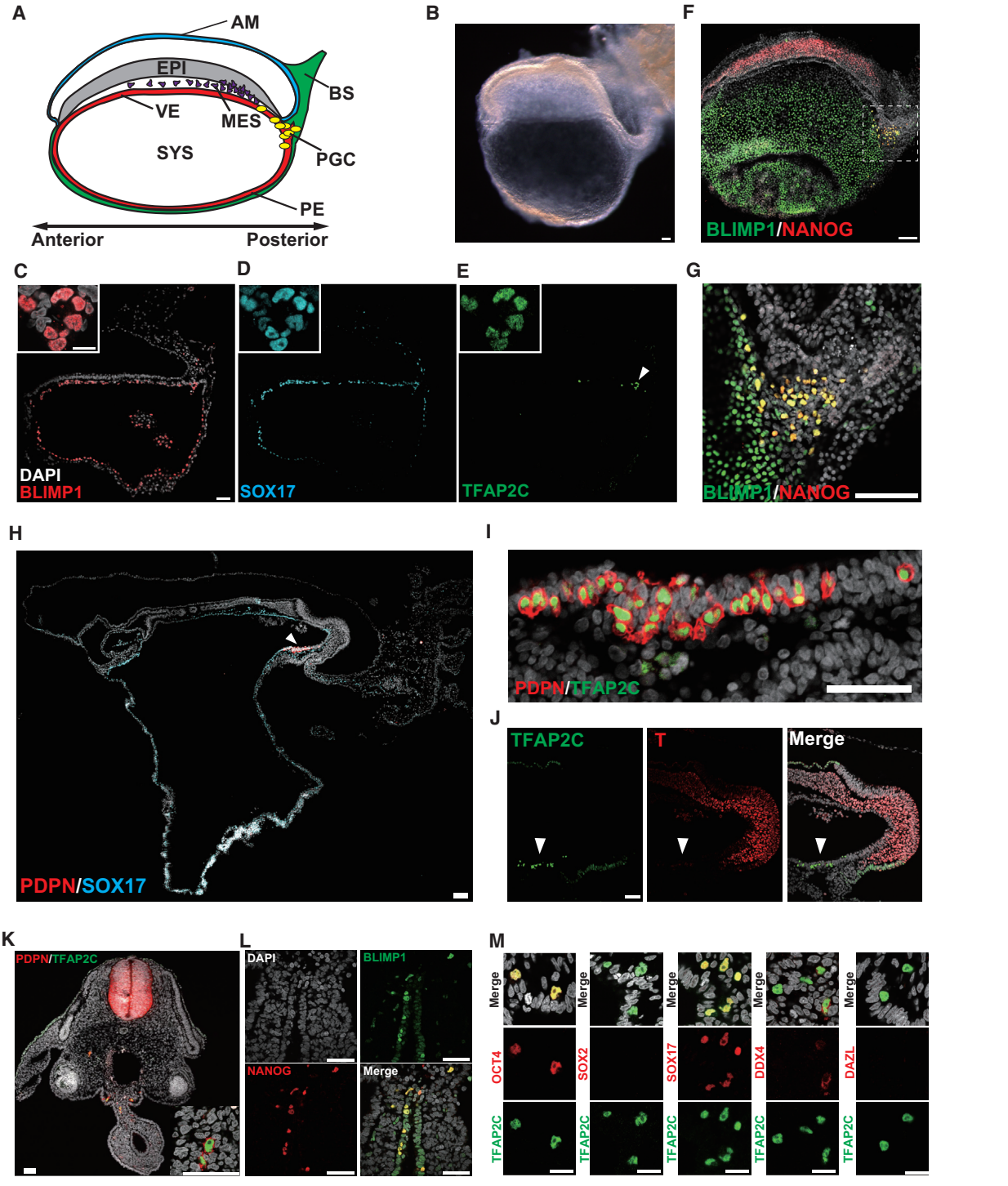

Figure 1. cyPGCs at Migration Stages

(A) Schematic of a cy embryo at E20. AM, amnion; BS, body stalk; EPI, epiblast; MES, mesoderm; PGC, primordial germ cells; VE, visceral endoderm; PE, parietal endoderm; SYS, secondary yolk sac.

(B) Lateral view of a cy embryo at E20. Scale bar, 50 μm.

(C–E) IF images of a cy embryo at E20 for DAPI and BLIMP1 (C), SOX17 (D), and TFAP2C (E). Scale bar, 50 μm. Insets show the higher magnifications of the area indicated by an arrowhead in (E). Scale bar, 10 μm.

(F) A single confocal section of a cy embryo at E21 stained as whole mount for BLIMP1 (green), NANOG (red), and DAPI (white). Scale bar, 100 μm.

(G) A magnified view of the region outlined by the dotted box in (F).

(legend continued on next page)

specification is significantly different from that of mouse embryos, and the direct extrapolation of the findings in mice to the mechanism for primate PGC specification may not necessarily be straightforward. This poses a significant limitation to studies of, for example, induction of the germ cell fate from primate pluripotent stem cells (PSCs) (Saitou and Miyauchi, 2016).

With ethical approval, we here set out to investigate germ cell development in primates using cynomolgus monkeys (cy; *Macaca fascicularis*) as a model (Nakamura et al., 2016; Sasaki et al., 2015; Yamasaki et al., 2011), and identified the origin of cyPGCs in the nascent amnion and the potential signaling mechanism for cyPGC specification.

RESULTS

cy Germ Cells in Embryonic/Fetal Gonads

We first characterized the properties of cyPGCs that colonized embryonic/early fetal gonads from E36 to E55 (Carnegie stage [CS] 17–23 and early fetal [O'Rahilly and Müller, 1987], corresponding roughly to E9.5–E12.5 in mice) (Figure S1A). During this period, cyPGCs showed constant morphologic characteristics: they were large in size, exhibited clear cytoplasms and large cleft nuclei with no evident heterochromatin, and typically had single prominent nucleoli (Figures S1B–S1F). Immunofluorescence (IF) analysis revealed that such cells were low for DAPI intensity and were positive ($^+$) for BLIMP1 and TFAP2C, key TFs for PGCs (Figures S1E–S1G) (Eckert et al., 2008; Irie et al., 2015; Ohinata et al., 2005; Pauls et al., 2005; Sasaki et al., 2015; Vincent et al., 2005; Weber et al., 2010). cyPGCs during this period were positive for pluripotency factors (OCT4 [also known as POU5F1], NANOG, SALL4, UTF1, LIN28A), RNA-binding proteins for germ cells (DDX4 [also known as VASA], DAZL), and SOX17, a TF critical for endoderm development and human PGC-like cell (hPGCLC) specification in vitro (Figure S1G) (Irie et al., 2015; Seguin et al., 2008). GATA4, a key TF for endoderm as well as gonad development (Hu et al., 2013; Soudais et al., 1995), exhibited robust and weak expression in Sertoli/granulosa cell precursors and cyPGCs, respectively (Figure S1G). Consistent with the observation in hPGCs (de Jong et al., 2008; Perrett et al., 2008), cyPGCs were negative ($^-$) for SOX2 (Figure S1G). Moreover, we identified the expression of a number of surface markers (TRA-1-60, TRA-1-81, PDPN, KIT) in cyPGCs (Figure S1G). Collectively, these findings establish the properties of cyPGCs in embryonic/early fetal gonads.

We were able to obtain several late-stage male embryos, including aborted ones (E70, E100, E110, and E124). Fetal seminiferous tubules with clear lumina were well established by E70 (Figure S1H), and essentially all male germ cells appeared positive for DDX4 at least until E124 (Figures S1G and S1I). At E70, around half of the DDX4$^+$ germ cells became negative for OCT4, NANOG, and TFAP2C, as well as for Ki-67, an antigen for proliferating cells (Gerdes et al., 1984) (Figures S1I and S1J). PLZF, a marker for (pro)spermatogonia in mice (Buaas et al., 2004; Costoya et al., 2004), began to be expressed in some germ cells as early as E50, and became positive in nearly 80% of germ cells at E70 (Figures S1I and S1J). By E124, nearly all the germ cells expressed PLZF, repressed OCT4, NANOG, LIN28A, BLIMP1, and TFAP2C, and were negative for Ki-67 (Figures S1I and S1J). Thus, after around E50 male cyPGCs progress gradually into mitotic arrest to differentiate into prospermatogonia, which is preceded by/coincident with the upregulation of PLZF and the repression of key PGC markers. Notably, however, even at E124, ~70%–80% of prospermatogonia continued to express SOX17 and SALL4 (Figures S1I and S1J), indicating their retention of some PGC properties and of potential heterogeneity.

cyPGCs during Migration

Politzer and Witschi provided histological observations on putative hPGCs as early as late week 3 within the posterior yolk sac endoderm (Politzer, 1930, 1933; Witschi, 1948). Recent studies have reported transcriptional and epigenetic properties of migrating hPGCs as early as week 4 (CS ~13) (Gkountela et al., 2015; Guo et al., 2015; Tang et al., 2015). However, there has been no detailed characterization of PGCs earlier than the migration stages in humans or primates (approximately week 4). Based on the validated markers (combinatorial detections among SOX17, TFAP2C, BLIMP1, OCT4, NANOG, and PDPN), we next characterized cyPGCs at the migration stages (E20–E28).

cy embryos isolated at E20 or E21 were in the pre-somite stages (CS 8) and exhibited prominent primitive streaks and developing body stalks linking the embryos with the chorionic plates (Figures 1A and 1B). In such embryos, while BLIMP1 was expressed uniformly in the VE and PE of the secondary yolk sac, SOX17 showed preferential expression in the VE: the cyPGCs, which were also positive for TFAP2C, NANOG, PDPN, or OCT4, were localized predominantly within/around the posterior PE, particularly at the base of the incipient allantoic diverticulum (embryos: n = 3; cyPGCs: 193/250, ~77%) (Figures 1C–1G, S2A, and S2B). A minor portion of cyPGCs were also present within the body stalk mesenchyme/posterior embryonic mesoderm (37/250, ~15%), or posterior VE (19/250, ~8%) (Figure S2B). An embryo isolated at E24 was in a somite stage (nine somites identified: CS 10) and nearly all the cyPGCs were within

(H) IF images of a cy embryo at E24 for PDPN (red) and SOX17 (cyan) merged with DAPI (white). An arrowhead indicates the emerging hindgut endoderm with colonized cyPGCs. Scale bar, 100 μm.

(I) A magnified view of the region indicated by an arrowhead in (H) stained with PDPN (red) and TFAP2C (green) merged with DAPI (white). Scale bar, 100 μm.

(J) IF images of the posterior part of a cy embryo at E24 (neighborhood section of H) for TFAP2C (green) or T (red) with a merge with DAPI (white). Arrowheads indicate cyPGCs as in (H). Note that TFAP2C is also weakly positive in the ectoderm. Scale bar, 50 μm.

(K) IF images of a cy embryo at E28 for PDPN (red) and TFAP2C (green) merged with DAPI (white). The inset shows a higher magnification of the area of the dorsal mesentery with two cyPGCs. Note that PDPN is also expressed in the neural tube. Scale bars, 50 μm.

(L) IF images of a cy embryo at E28 (different from that in J) for BLIMP1 (green) and NANOG (red) merged with DAPI (white), highlighting cyPGCs within the hindgut endoderm and surrounding mesenchyme. Scale bars, 50 μm.

(M) IF analysis for the expression of OCT4, SOX2, SOX17, DDX4, or DAZL (red) in the TFAP2C$^+$ (green) migrating cyPGCs at E28. Merges with DAPI (white) are shown at the top. Scale bars, 20 μm.

See also Figures S1, S2, and S7.

Please cite this article in press as: Sasaki et al., The Germ Cell Fate of Cynomolgus Monkeys Is Specified in the Nascent Amnion, Developmental Cell (2016), http://dx.doi.org/10.1016/j.devcel.2016.09.007

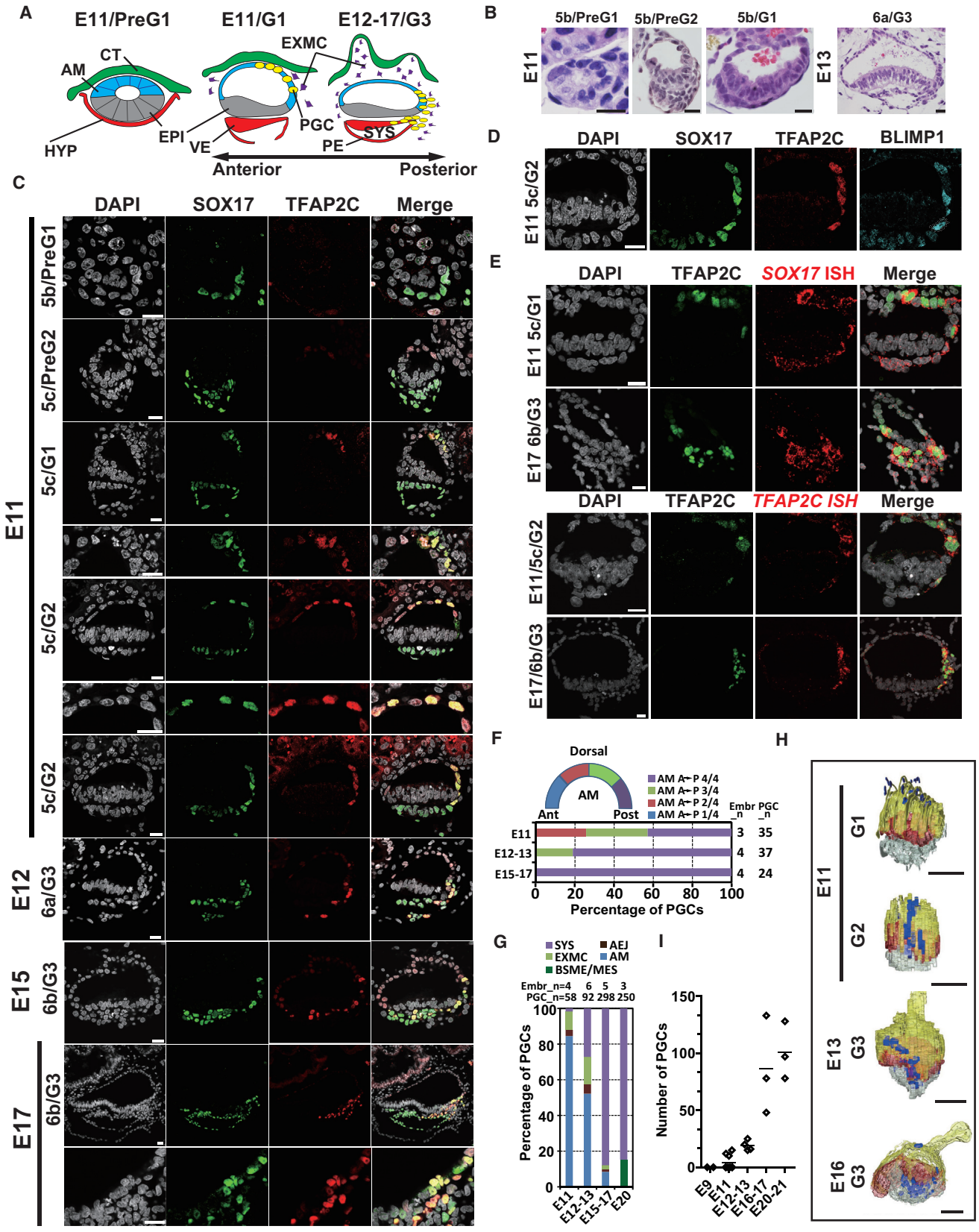

(legend on next page)

the emerging hindgut endoderm, which was incorporated in the body cavity of the embryo proper upon embryo folding (Figures 1H–1J).

At E28, cy embryos (n = 2) were in a post-somite stage (CS 13), and cyPGCs were present either in the hindgut endoderm (42/310, ~14%) or mesenchyme (36/310, ~12%), the dorsal wall of the mesentery (69/310, ~22%), or bilateral coelomic angles, namely, the anlage of the gonads (159/310, ~51%) (Figures 1K, 1L, S2C, and S2D). Although previous studies have reported that hPGCs migrate along nerve fibers (Hoyer et al., 2005; Mamsen et al., 2012), we did not find evidence of such migration in cy embryos at this stage by co-staining with cyPGC markers and βIII-tubulin (Figures S2C and S2D). At day 36, a cy embryo (n = 2) was in a post-somite stage (CS 17) and, as described above, a majority of cyPGCs (350/575, ~61%) colonized the gonads (Figure S1G), while a minority of them were still present within the dorsal mesentery (127/575, ~22%) or aorta-gonad-mesonephros regions outside the gonads (89/575, ~15%) (data not shown). It is noteworthy that, although cyPGCs during migration expressed most of the markers validated in gonadal cyPGCs, they were negative for DDX4 and DAZL: cyPGCs began to express DDX4 from around E28 and did not show DAZL throughout weeks 3–4 (Figure 1M). In addition, cyPGCs were consistently negative for SOX2 (Figures 1M and S2B). Together, these findings define the migratory pathway of cyPGCs from the base of the allantoic diverticulum to the developing gonads.

The Origin of cyPGCs

We set out to determine the origin of cyPGCs in early post-implantation embryos (from E11 to E17) (Figure S3; Nakamura et al., 2016). Consistent with the previous literature (Enders and King, 1988; Enders et al., 1986; Heuser and Streeter, 1941; Luckett, 1978), by dissection microscopy and histological examination, we detected the formation of the amniotic cavity at E11, formation of the secondary yolk sac at E11–E12, formation of the anterior-to-posterior axis (formation of columnar anterior VE) at E11–E13, and onset of gastrulation (marked proliferation of cells at the posterior junction of the epiblast and the VE) at E13–E14 (Figures 2A, 2B, and S3A–S3D; see Figures S3E–S3K for key developmental indices and the distributions of developmental stages of isolated embryos).

As potential markers for nascent cyPGCs, we used SOX17 and TFAP2C, since they exhibited strong expression in migrating cyPGCs (Figures 1 and S2) and showed acute and robust upregulation upon induction of hPGCLCs from hPSCs in vitro (Irie et al., 2015; Sasaki et al., 2015). Note that while both SOX17 and BLIMP1 were also expressed in the endoderm, TFAP2C was more specific to cyPGCs (Figures 1 and S2). In hatching blastocysts cultured in vitro for 9 days (E9) (n = 3) (Nakamura et al., 2016), we did not detect cells co-expressing SOX17 and TFAP2C (Figure S4A). In half of the post-implantation embryos isolated at E11 (5/10, 50%) (PreG1 and PreG2 stages [Figures 2A–2C and S3K]), SOX17 was specifically expressed in VE and TFAP2C was barely detectable/only weakly positive in the amnion (Figure 2C): We did not detect SOX17/TFAP2C doubly positive cells in serial sections of these embryos. Note that the amnion began to acquire cuboidal/squamous morphology from the PreG2 stage onward (Figures 2B, 2C, and S3C). Strikingly, however, in the remaining five embryos with relatively advanced stages (G1 or G2 stage [Figures 2A, 2C, and S3K], 5/10, 50%), we identified a number of SOX17/TFAP2C doubly positive cells at the dorsal amnion juxtaposed with the cytotrophoblast layer of the developing placenta (Figures 2A and 2C): the SOX17/TFAP2C^{+} cells were scattered around the dorsal amnion in three of the five embryos and were located in the posterior half of the amnion in the two more advanced embryos (Figure 2C). Notably, SOX17/TFAP2C strongly positive cells were intermingled with SOX17 strongly positive/TFAP2C$^{+/-}$ or SOX17$^{+/-}$/TFAP2C strongly positive cells (Figure 2C), and also exhibited a variable level of BLIMP1 (Figure 2D), suggesting that cyPGC specification is in progress in these cells. We performed in situ hybridization (ISH) of *SOX17* and *TFAP2C* mRNA followed by IF analysis of TFAP2C on

Figure 2. cyPGC Specification in the Amnion

(A) A schematic summary of cyPGC specification in the amnion. CT, cytotrophoblast; HYP, hypoblast; EXMC, extra-embryonic mesenchyme. Other abbreviations for embryonic cell types are as in Figure 1A. Embryonic stages are defined as follows: PreG1, cy embryos with a small AM cavity surrounded by less than 15 EPI/AM cells per cross-section and with no cyPGCs (SOX17/TFAP2C^{+}); PreG2, cy embryos with a larger AM cavity surrounded by more than 15 EPI/AM cells per cross-section and with no cyPGCs; G1, cy embryos with morphologic characteristics similar to PreG2, but with cyPGCs; G2, cy embryos with at least one cyPGC migrated beneath EPI, but no cyPGCs within VE/PE; G3, cy embryos with cyPGCs within VE/PE.

(B) Representative sections of cy embryos at the indicated stages stained by H&E. Embryonic days and stages (left, Carnegie stage; right, cyPGC-based stage) are indicated. Scale bars, 20 μm.

(C) IF images of paraffin sections of cy embryos at the indicated stages for SOX17 (green), TFAP2C (red), and DAPI (white), with their merges. Sagittal sections (anterior, left; posterior, right) are shown when embryos exhibited an appreciable AP axis. For some embryos, regions with cyPGCs are magnified. Scale bars, 20 μm.

(D) IF images of paraffin sections of cy embryos at E11 for DAPI (white), SOX17 (green), TFAP2C (red), and BLIMP1 (cyan). Scale bar, 20 μm.

(E) Images for combined in situ hybridization (co-ISH) for *SOX17* (top) or *TFAP2C* (bottom) (red) with IF for TFAP2C (green) on paraffin sections of cy embryos at E11 or E17. Merged images with DAPI (white) are also shown (far right). Scale bars, 20 μm.

(F) Distributions of cyPGCs within the AM at the indicated stages. The AM was separated into quadrants (anterior/proximal, blue; anterior/distal, red; posterior/distal, green; posterior/proximal, purple), and the frequencies of cyPGCs in each compartment are shown. Numbers of embryos and cyPGCs analyzed at the indicated stages are shown on the right.

(G) Distributions of cyPGCs within the indicated regions at the indicated stages. AEJ, amnion-epiblast junction. Other abbreviations are as in (A) and Figure 1A. BSME for E20 embryos indicates the extra-embryonic mesoderm within the BS. Numbers of embryos and cyPGCs at the indicated stages are shown above the graph.

(H) Posterior views of three-dimensional reconstructions of the sections of representative embryos at the indicated stages. Embryos were colored as follows: AM, yellow; EPI, red; VE/PE, white; PGCs, blue. Scale bars, 50 μm.

(I) Numbers of cyPGCs counted on serial sections stained with TFAP2C and SOX17 at the indicated stages. Bars indicate mean values.

See also Figures S3–S5 and S7.

Please cite this article in press as: Sasaki et al., The Germ Cell Fate of Cynomolgus Monkeys Is Specified in the Nascent Amnion, Developmental Cell (2016), http://dx.doi.org/10.1016/j.devcel.2016.09.007

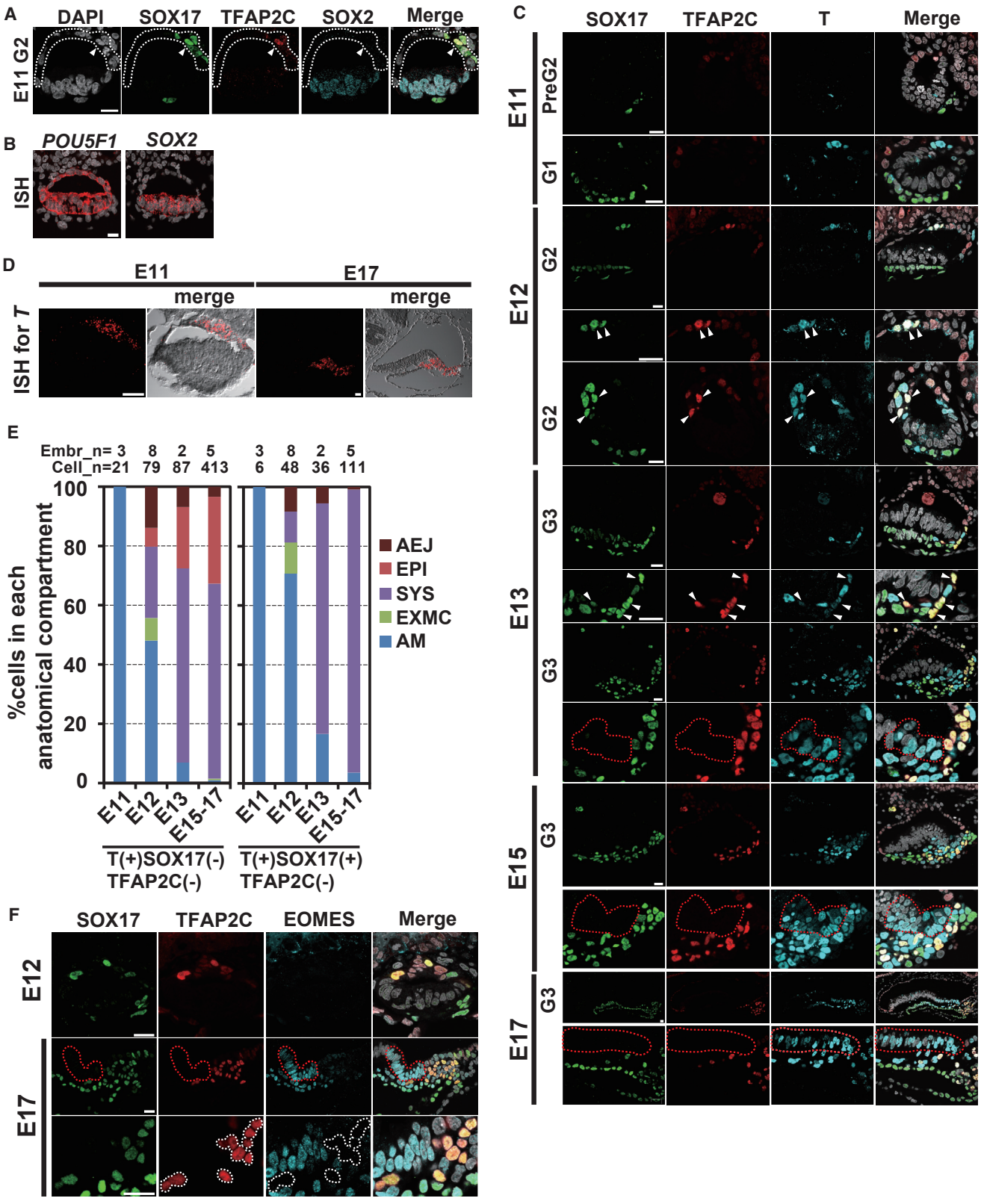

(legend on next page)

embryos at E11, which validated the robust expression of *SOX17* and *TFAP2C*/TFAP2C in the dorsal amnion (Figure 2E).

At E12–13, all embryos bore SOX17/TFAP2C doubly positive cells predominantly within the amnion, with their primary location being shifted toward the posterior quadrant (G2 and G3 stages [Figures 2C and 2F]). Notably, some of the SOX17/TFAP2C/BLIMP1$^+$ cells were present in the space between the posterior amnion and underlying extra-embryonic mesenchyme or beneath the posterior epiblast (Figures 2C, 2G, and S4B), suggesting that the SOX17/TFAP2C/BLIMP1$^+$ cells in the amnion exhibited migration. Consistently, the basement membrane was broken down and the SOX17/TFAP2C$^+$ cells appeared to undergo epithelial-mesenchymal transition (EMT) with positivity for VIMENTIN around such locations (Figure S4C). At E15–E17, the SOX17/TFAP2C$^+$ cells were still present within the posterior amnion, particularly around the junction between the amnion and epiblast, but were most prevalent between the posterior epiblast and VE, and within VE (G3 stage), where they exhibited a completion of the EMT (VIMENTIN$^+$/CDH1$^-$) (Figures 2A, 2C, 2F, 2G, S4C, and S4D). Note that, throughout the period examined (from E11 to E17), we did not detect cyPGCs (SOX17/TFAP2C doubly positive cells) or cells that appeared to be in the process for cyPGC specification (SOX17$^+$/TFAP2C$^-$ or SOX17$^-$/TFAP2C$^+$ cells) within the epiblast.

We next examined the cell-cycle state of cyPGCs. The TFAP2C$^+$ cells in the dorsal amnion at G1 at E11 were positive for Ki-67 (Figure S4E). At E17, a majority of the amnion was negative for Ki-67 except for the cells at the posterior amnion, including the TFAP2C$^+$ cells (Figure S4E), indicating that cyPGCs are in a proliferating state in the amnion.

We three-dimensionally reconstituted the sections of embryos at E11, E13, and E16 for SOX17/TFAP2C expression, which delineated the specification and initial migration of cyPGCs (Figure 2H): cyPGCs are specified at the dorsal amnion in a scattered fashion (about ten in number at E11), migrate down along the posterior midline of the amnion toward the VE or continue to be specified at the posterior amnion, and expand substantially in number between the posterior epiblast and VE (~90 in number at E16–E17) (Figures 2H and 2I). Note that delamination/migration of cyPGCs within/from the amnion occurs prior to the onset of gastrulation (see below).

cyPGC Specification and Key Pluripotency Factors

We explored the relationship between cyPGC specification and the expression of key pluripotency factors. The two embryos at PreG1 at E11 exhibited uniform expression of OCT4, SOX2, and NANOG both in the epiblast and amnion (Figures S5A–S5D), indicating that the nascent amnion bears gene expression properties similar to those of the epiblast. The embryos at PreG2 (n = 2) continued to express OCT4 and NANOG throughout the amnion, but downregulated SOX2, apparently first from the dorsal amnion and then throughout the amnion (Figures S5A–S5D). Accordingly, the two embryos at G1 at E11 were positive for OCT4 and NANOG, but negative for SOX2 in the amnion (Figures S5A–S5D). The analysis of an embryo at G2 at E11 clearly demonstrated that SOX17/TFAP2C$^+$ cells are induced in the amnion negative for SOX2 (Figure 3A). An ISH analysis of another embryo at the same stage revealed that *SOX2*, but not *POU5F1*, mRNA was downregulated at the transcription level (Figure 3B). These findings indicate that upon cyPGC specification, the POU5F1/SOX2/NANOG$^+$ amnion downregulates SOX2 and acquires SOX17 and TFAP2C, which is consistent with a rapid downregulation of SOX2 upon hPGCLC specification from hPSCs (Irie et al., 2015; Sasaki et al., 2015). Notably, cyPGCs in the amnion at G2 at E11, as well as the epiblast, expressed *PRDM14*, a key regulator for naive pluripotency and mPGC specification (Figure S5E) (Yamaji et al., 2008, 2013).

After E12, OCT4 and NANOG were gradually downregulated from the amnion, except for cyPGCs and the most posterior portion of the amnion contiguous with the epiblast, where OCT4 and NANOG persisted at least until E17, but waned by E20 (Figures S5A–S5D). Combined with the analysis of the cell-cycle state of cyPGCs (Figure S4E), these findings indicate that cyPGC specification at the dorsal amnion is a transient event and that cyPGC specification may continue at the posterior amnion. In contrast, OCT4/SOX2/NANOG remained highly expressed in the epiblast at least until E20, with rapid downregulation of SOX2 in gastrulating cells (embryos: n = 2; Figure S5C) (Nakamura et al., 2016). Thereafter, the three factors were downregulated by E24 (embryos: n = 1; early somite stage, CS 10), except in the neural tube, where SOX2 showed strong expression (Figure S5G and data not shown). *PRDM14* continued to be expressed in the epiblast at least until E17 and in cyPGCs until E36 (Figure S5F).

cyPGC Specification and T, a Key "Mesodermal" TF

T, a key "mesodermal" TF, activates *Blimp1* and *Prdm14*, and is essential for mPGC specification (Aramaki et al., 2013). *T* is also accompanied by hPGCLC specification (Irie et al., 2015; Sasaki et al., 2015). We therefore examined whether T might also be associated with cyPGC specification in the amnion.

Figure 3. cyPGC Specification Accompanies T Expression

(A) IF images of the paraffin sections of cy embryos at E11 for SOX17 (green), TFAP2C (red), and SOX2 (cyan) with a merge with DAPI (white). White arrowheads indicate cyPGCs. The amnion, as distinguished from the underlying EPI by SOX2 negativity, is outlined by white dotted lines. Scale bar, 20 μm.

(B) ISH images of paraffin sections of cy embryos at E11 for *POU5F1* (left) or *SOX2* (right) (red), with merges with DAPI (white). Scale bar, 20 μm.

(C) IF images of paraffin sections of cy embryos at E11–E17 for SOX17 (green), TFAP2C (red), and T (cyan), with merges with DAPI (white). cyPGC-based stages are indicated at the left. Sagittal sections (anterior, left; posterior, right) are shown when embryos exhibited an appreciable AP axis. For some embryos, regions with cyPGCs are magnified. White arrowheads and red dotted lines indicate cyPGCs and posterior EPI with T reactivity (presumptive nascent primitive streak), respectively. Scale bars, 20 μm.

(D) Images for ISH of *T* on paraffin sections of cy embryos at the indicated stages. Merged images of *T* (red) and bright fields are shown. Scale bars, 50 μm.

(E) Distributions of T$^+$/SOX17$^-$/TFAP2C$^-$ or T$^+$/SOX17$^+$/TFAP2C$^-$ cells within the indicated regions at the indicated stages. Abbreviations are as in Figures 1A, 2A, and 2G. Numbers of embryos and analyzed cells at the indicated stages are shown above the graph.

(F) IF images of the paraffin sections of cy embryos at E12 and E17 for SOX17 (green), TFAP2C (red), and EOMES (cyan) with merges with DAPI (white). EPI with EOMES reactivity and cyPGCs are outlined by red and white dotted lines, respectively. Scale bars, 20 μm.

See also Figures S3–S5 and S7.

Please cite this article in press as: Sasaki et al., The Germ Cell Fate of Cynomolgus Monkeys Is Specified in the Nascent Amnion, Developmental Cell (2016), http://dx.doi.org/10.1016/j.devcel.2016.09.007

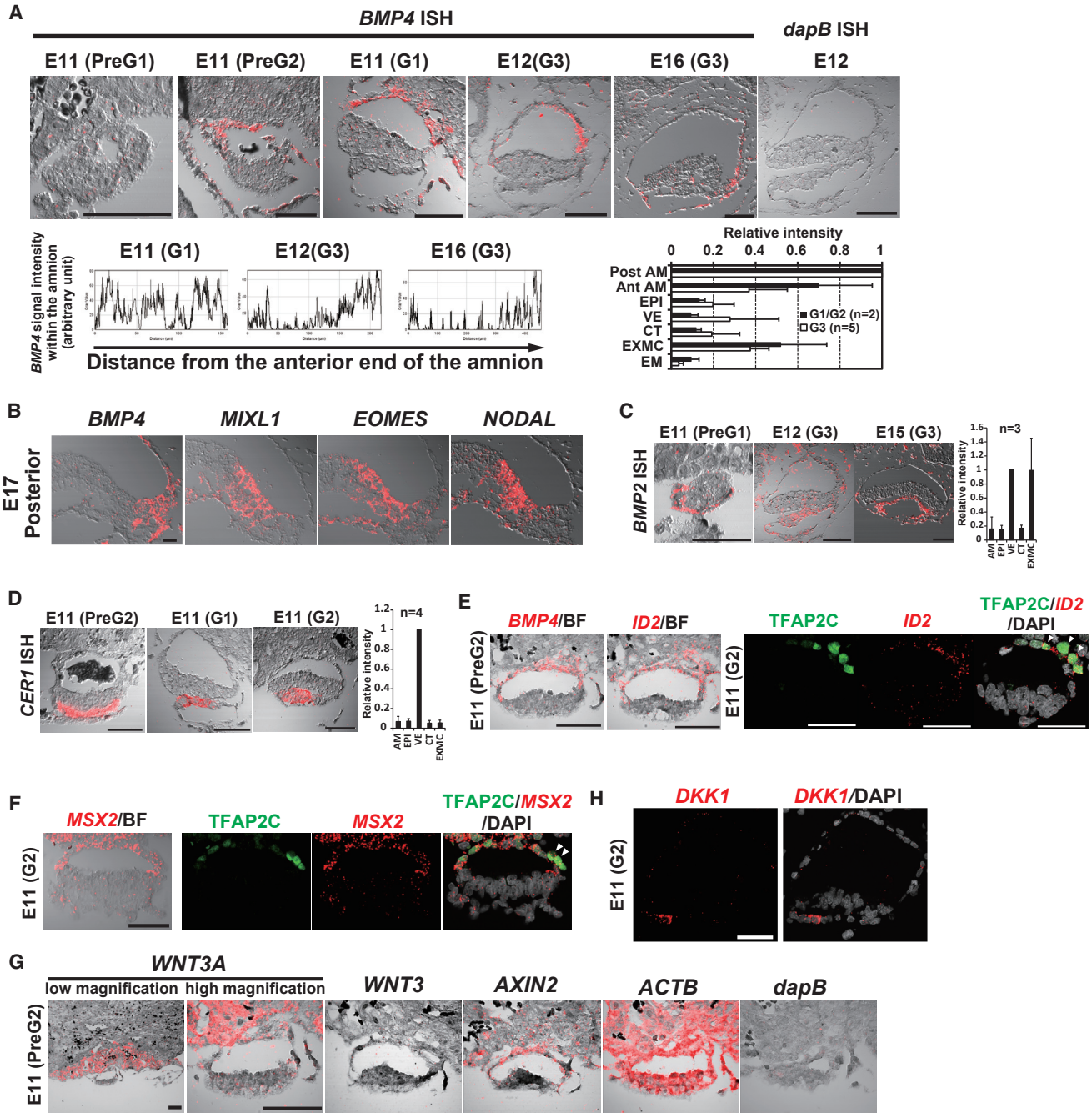

Figure 4. Expression of Signaling Molecules in cy Embryos

(A) (Top) ISH of *BMP4* (left) or *dapB* (negative control, far right) on paraffin sections of cy embryos at the indicated stages. Merged images of *BMP4* (red) and bright fields are shown. Scale bars, 50 μm. (Bottom left) Signal intensities of *BMP4* within AM. x Axis denotes distance (μm) from the anterior end of AM. (Bottom right) Relative signal intensities of *BMP4* within the indicated cells at the indicated stages between E11 and E17. The average signal intensities of the posterior half of AM were set as 1. Averages with SDs of two or five embryos are shown.

(B) ISH of *BMP4*, *MIXL1*, *EOMES*, and *NODAL* on serial sections (near midline) of sagittally oriented cy embryos at E17. Merged images with bright fields on the posterior part of the embryos are shown. Scale bar, 20 μm.

(C) (Left) ISH of *BMP2* at the indicated stages. Scale bars, 50 μm. (Right) Relative signal intensities of *BMP2* within the indicated cells. The average signal intensities of VE were set as 1. Averages with SDs of three embryos (E12–E16) are shown.

(D) (Left) ISH of *CER1* at the indicated stages. Scale bars, 50 μm. (Right) Relative signal intensities of *CER1* within the indicated cells. The average signal intensities of VE were set as 1. Averages with SDs of four embryos at E11 (G1, G2) are shown.

(E) ISH images for *BMP4* or *ID2* (red) merged with bright field (left) or co-ISH/IF images for *ID2* (red) and TFAP2C (green) with a merge with DAPI (white) (right) on cy embryos at E11. Arrowheads indicate TFAP2C^{+} cyPGCs. Scale bars, 50 μm.

(legend continued on next page)

We did not detect T at PreG2 at E11 (Figure 3C). Remarkably, however, in a section of an embryo at G1, we detected T in a few cells negative for SOX17/TFAP2C at the dorsal amnion (Figure 3C). Moreover, in a section of an embryo at G2 at E12, we detected specific expression of T in SOX17/TFAP2C doubly positive cells in the dorsal amnion, while no cells in the epiblast exhibited T (Figure 3C). In a section of another G2 embryo at E12, we detected T in SOX17/TFAP2C$^+$ cells, SOX17$^+$/TFAP2C$^-$ cells, and SOX17$^-$/TFAP2C$^-$ cells within the amnion (Figure 3C). In good agreement with these observations, an ISH analysis demonstrated that at G1 at E11, *T* mRNA was strongly expressed exclusively in the amnion, particularly around the dorsal area in close proximity to the cytotrophoblast layer of the developing placenta (Figure 3D). Thus, the dorsal amnion at E11/E12 expresses T in a widespread fashion.

In some other embryos at G2 at E12, while T$^+$ cells were located predominantly in the amnion, we detected a few T$^+$/SOX17$^-$/TFAP2C$^-$ cells in the posteriormost epiblast and between the epiblast and VE, or T$^+$/SOX17$^+$/TFAP2C$^-$ cells in between the epiblast and VE (Figure 3E). In embryos at the E13 (G3 stage), we detected T$^+$/SOX17$^-$/TFAP2C$^-$ cells in the posterior epiblast, presumably at the early primitive streak (red dotted area in Figure 3C) and between the epiblast and VE, or T$^+$/SOX17$^+$/TFAP2C$^-$ cells predominantly between the epiblast and VE (Figures 3C and 3E). Compared with such cells, SOX17/TFAP2C$^+$ cyPGCs were only weakly positive for T (Figure 3C). The T$^+$ cells either positive or negative for SOX17 that appear from late E12 or E13 beneath the epiblast would be either cells that migrated down from the amnion or incipient gastrulating mesoderm cells from the epiblast (Nakamura et al., 2016). Collectively, these findings indicate that at E11, cells in the amnion, including SOX17/TFAP2C$^+$ cyPGCs, initiate T expression prior to and independently from onset of gastrulation in the epiblast, and at around late E12, the epiblast begins gastrulation to generate mesoderm/endoderm.

At E15 and E17, T was expressed in the primitive streak (red dotted area in Figure 3C), where the basement membrane was disrupted, and more strongly in meso-/endodermal cells beneath the epiblast: the great majority of the amnion at these embryos lacked T expression (Figures 3C and 3E). Meanwhile, cyPGCs were only weakly positive for T at these stages and generally located away from the disrupted basement membrane beneath the epiblast (Figure 3C). Unlike in the amnion, we did not observe SOX17 and/or TFAP2C$^+$ cells, a potential precursor state of cyPGCs, in the posterior epiblast, although beneath the epiblast, we found numerous SOX17$^+$/TFAP2C$^-$/T$^+$ cells, which presumably represent precursors for the definitive endoderm (Figures 3C and 3E). ISH revealed that *T* showed specific and robust expression in the primitive streak and gastrulating mesoderm at E17 (Figure 3D). These findings support the possibility that cyPGCs originate solely from the amnion (initially from the dorsal and later from the posterior amnion), but not from the epiblast after segregation of the amnion. In further support of this notion, we did not detect EOMES, another early meso-/endodermal marker (Russ et al., 2000), in the SOX17/TFAP2C$^+$ cells in a G1 embryo at E12, whereas we found strong EOMES positivity in the primitive streak (red dotted area in Figure 3F) and gastrulating cells, but not cyPGCs (white dotted cells in Figure 3F), at E17. Combined with the observation that cyPGCs appear to undergo delamination and migration from the dorsal to the posterior amnion and then beneath the epiblast (Figures 2 and S4C), our data suggest the unique cellular dynamics and gene expression associated with cyPGC specification in the amnion.

Amnion as an Autocrine Signaling Center for cyPGC Specification

We next sought a potential signaling mechanism for cyPGC specification by examining the expression of a number of signaling molecules, their antagonists, and their targets, which would be potentially relevant for cyPGC specification. We first examined the expression of *BMP4*, a key cytokine for mPGC specification (Lawson et al., 1999; Ohinata et al., 2009; Saitou et al., 2002) and m/hPGCLC induction (Hayashi et al., 2011; Irie et al., 2015; Sasaki et al., 2015). In a PreG1 embryo at E11, although the extra-embryonic mesenchyme exhibited weak *BMP4* expression, no other cells showed *BMP4* (Figure 4A). Strikingly, however, in one PreG2 and one G1 embryo at E11, we identified strong *BMP4* expression throughout the amnion (Figure 4A). *BMP4* continued to show robust expression in the amnion, but its expression domain shifted proximally and to some extent posteriorly in embryos at E12 and E16 (Figures 4A and 4B). Thus, the expression of *BMP4* in the amnion precedes the emergence of SOX17/TFAP2C$^+$ cyPGCs and continues thereafter in the amnion.

An embryo at E16 also exhibited *BMP4* in some gastrulating cells (Figures 4A and 4B). Notably, analyses of serial sections revealed that *BMP4* exhibited a unique pattern of expression in the proximal/posterior amnion, the junction between the amnion and epiblast, and some delaminating/gastrulating cells, which were distinct from the primitive streak and mesodermal cells expressing *MIXL1*, *EOMES*, and *NODAL* (Figure 4B). At E24, *BMP4* was restricted to the emerging heart tube and posterior extra-embryonic mesoderm, and became undetectable in the amnion (data not shown).

We next examined the expression of *BMP2*. In stark contrast to *BMP4*, we detected strong expression of *BMP2* in the VE in a PreG1 embryo at E11 (Figure 4C), and in the VE, PE, and extra-embryonic mesenchyme in embryos at E12 and E15, consistent with the notion that the VE generates the extra-embryonic mesenchyme (Figure 4C) (Enders and King, 1988; Luckett, 1978; Nakamura et al., 2016). We then found that *CER1*, an antagonist for BMP signaling (for review see Arnold and Robertson, 2009), was robustly expressed throughout the VE in a PreG2 embryo at E11 and in approximately the anterior two-thirds of VE in G1 and G2 embryos at E11 (Figure 4D). Thus, *CER1* is

(F) Co-ISH/IF images for *MSX2* (red) and TFAP2C (green) with merges with bright field (far left) or DAPI (white) (far right) on a cy embryo at E11. Arrowheads indicate TFAP2C$^+$ cyPGCs. Scale bar, 50 μm.

(G) ISH of *WNT3A*, *WNT3*, *AXIN2*, *ACTB* (positive control, second right), and *dapB* (negative control, far right) on serial sections of cy embryos at E11. Merged images with bright fields are shown. Scale bars, 50 μm.

(H) ISH for *DKK1* on a section of a cy embryo at E11. A merge with DAPI (white) is shown. Scale bar, 50 μm.

expressed in cells located almost diagonally to nascent cyPGCs in embryos at this stage. Importantly, *ID2* and *MSX2*, key immediate targets of BMP signaling (Aramaki et al., 2013; Hollnagel et al., 1999), were expressed almost exclusively in the amnion and cyPGCs (*MSX2* was also expressed weakly in VE), but not in the epiblast (Figures 4E and 4F), suggesting that it is primarily the amnion that responds to BMP signaling.

We next examined the expressions of *WNT3* and *WNT3A*, the former of which is essential for mPGC(LC) induction (Aramaki et al., 2013; Ohinata et al., 2009). Although we could not detect *WNT3* in the embryos examined, we found robust expression of *WNT3A*, a molecule highly similar to *WNT3*, throughout the developing placenta, including the cytotrophoblast layer close to the amnion as well as in the amnion itself, in an embryo at E11 (Figure 4G). Notably, *DKK1*, an antagonist of WNT signaling (for review see Arnold and Robertson, 2009), was expressed in the anterior VE (Figure 4H), while *AXIN2*, one of the immediate targets of WNT signaling (Hamada et al., 1999), was expressed robustly in the amnion, but not in the epiblast, in an embryo at E11 (Figure 4G). This suggests that the amnion, but not the epiblast, primarily responds to both BMP4 and WNT signaling in embryos at this stage. Thus, BMP4 and WNT3A may act as autocrine signals for inducing cyPGCs in the amnion, and inhibitors such as CER1 and DKK1 prohibit cyPGC specification within the epiblast and anterior amnion.

cyPGCs Acquire a Unique Transcriptome

Having established the origin and the developmental pathway of cyPGCs, we next determined the transcriptome of cyPGCs during their development. As reported recently (Nakamura et al., 2016), we prepared single-cell cDNAs from post-implantation cy embryos using the single-cell mRNA 3′-end sequencing (SC3-seq) method (Nakamura et al., 2015). To isolate cyPGCs that exist only in a small number per embryo, we manually dissected out embryonic fragments expected to contain cyPGCs (E13, one embryo; E14, two embryos; E16, embryos; E17, two embryos; E20, one embryo), and generated 57, 99, 138, 183, and 77 cDNAs of appropriate quality from E13, E14, E16, E17, and E20 embryos, respectively (Figure S6A). We screened candidates for cyPGCs by the expression of *SOX17*, *TFAP2C*, *PRDM1* (gene name for BLIMP1), *PRDM14*, and *T*, and by the absence of *SOX2* (cyPGC candidates: E13, 3; E14, 0; E16, 7; E17, 4; E20, 1) (Figures S6A–S6C). We also generated six, one, and two cDNAs from cyPGCs (*POU5F1* [gene name for OCT4]/*NANOG*/*PRDM1*$^{+}$) of male embryonic gonads at E36, E47, and E55, respectively (Figures S6A and S6D), and as reported previously (Sasaki et al., 2015), we generated seven, five, and seven cDNAs from cyPGCs of female embryonic gonads at E43, E50, and E51, respectively. We analyzed the transcriptome of these cyPGC candidates/cyPGCs in comparison with those of cells in the cy epiblast lineages that we described recently (ICM [inner cell mass], pre-EPI [pre-implantation epiblast], postE- or L-EPI [post-implantation early or late epiblast], and Gast [gastrulating cells]) (Table S1) (Nakamura et al., 2016).

Unsupervised hierarchical clustering (UHC) revealed a tight clustering of cyPGC candidates isolated from early embryos (E13, E16, E17, and E20), which were in turn clustered closely with male cyPGCs at E36 and then with late male and female cyPGCs (Figure 5A), demonstrating their identity as early cyPGCs. Principal component analysis (PCA) showed that the identity of cyPGCs, including those at E13, the earliest cyPGCs that we isolated for the RNA-sequencing (RNA-seq) analysis, was distinct from that of other cell types in the epiblast lineage, including the epiblast and gastrulating cells at E13 (postE-EPI and Gast) (Figure 5B) (Nakamura et al., 2016). These findings are in accord with our observation that cyPGC specification occurs in the amnion as early as E11. We did not detect significant gene expression differences between male and female cyPGCs that we analyzed, in part due to the relatively small numbers of single-cell cDNAs we generated from similar developmental stages (data not shown).

We defined the 544 and 506 genes with significantly positive and negative scores for PC2 loading (SD >2) as cyPGC genes and non-cyPGC genes, respectively (Table S2). The cyPGC genes included genes potentially vital for cyPGCs, such as *SOX17*, *TFAP2C*, *PRDM1*, *KIT*, *NANOS3*, and *TFAP2L1*, and genes indicative of EMTs, such as *VIM*, *MMP2*, and *CDH2*, and were enriched with those bearing gene ontology (GO) functional terms for a number of unique developmental/signaling/metabolic pathways; whereas the non-cyPGC genes included genes such as *DNMT3A/3B*, *UHRF1*, *EHMT2*, *ZFP57*, *SOX2*, *CDH1*, and *GJA1*, and were enriched for GO terms characteristic of pre- and post-EPI, such as "mitochondrion" and "neuron development/neuron projection development," respectively (Figure 5B) (Nakamura et al., 2016).

Reflecting the repression of *DNMT3A/3B/UHRF1* and *EHMT2* in cyPGCs (Figures 5B and S6E), cyPGCs exhibited a reduction in global levels of 5-methylcytosine (5mC) and histone H3 lysine 9 dimethylation (H3K9me2) from as early as around E20 and appeared to exhibit unique epigenetic profiles (Figure S7), and all these changes are consistent with the epigenetic reprogramming in mice and humans (Gkountela et al., 2015; Guo et al., 2015; Kurimoto et al., 2015; Seki et al., 2005; Tang et al., 2015). Thus, cyPGCs acquire unique transcriptional properties upon their specification and development, which would be a basis for epigenetic reprogramming in cyPGCs.

cyPGCs Compared with hPGCLCs

hPGCLCs are induced from human PSCs, including embryonic stem cells and induced pluripotent stem cells (iPSCs), in vitro, and thus the identity of hPGCLCs should require further evaluation (Irie et al., 2015; Sasaki et al., 2015). We therefore compared the transcriptional properties of hPGCLCs (Sasaki et al., 2015) with those of cyPGCs of all developmental stages. The expression of key genes for germ cell development (*SOX17*, *PRDM1*, *TFAP2C*, *NANOS3*, *DPPA3*, *KIT*, *TCL1A*, *DDX4*, *DAZL*, *KRBOX1*, *RNF17*), pluripotency (*POU5F1*, *NANOG*, *SOX2*, *TFCP2L1*, *PRDM14*, *KLF4*), mesoderm/endoderm development (*T*, *MIXL1*, *SP5*, *GATA4*), EMT (*CDH1*, *CDH2*, *VIM*), and surface markers (*EPCAM*, *ITGA6*, *PDPN*, *CD38*, *ALPL* [also known as *TNAP*]) in hPGCLCs was highly consistent with that in cyPGCs, particularly early cyPGCs (Figures 6A and 6B). That is, hPGCLCs and early cyPGCs exhibited no/low expression of *DDX4*, *DAZL*, *DPPA3*, *KRBOX1*, and *RNF17*, whereas late cyPGCs expressed high levels of these genes, and hPGCLCs and some early cyPGCs expressed *CDH1* at relatively high levels, whereas late cyPGCs repressed *CDH1*. Note that, unlike hPGCLCs/hPGCs, cyPGCs did not show *CD38* (Figure 6B) (Irie

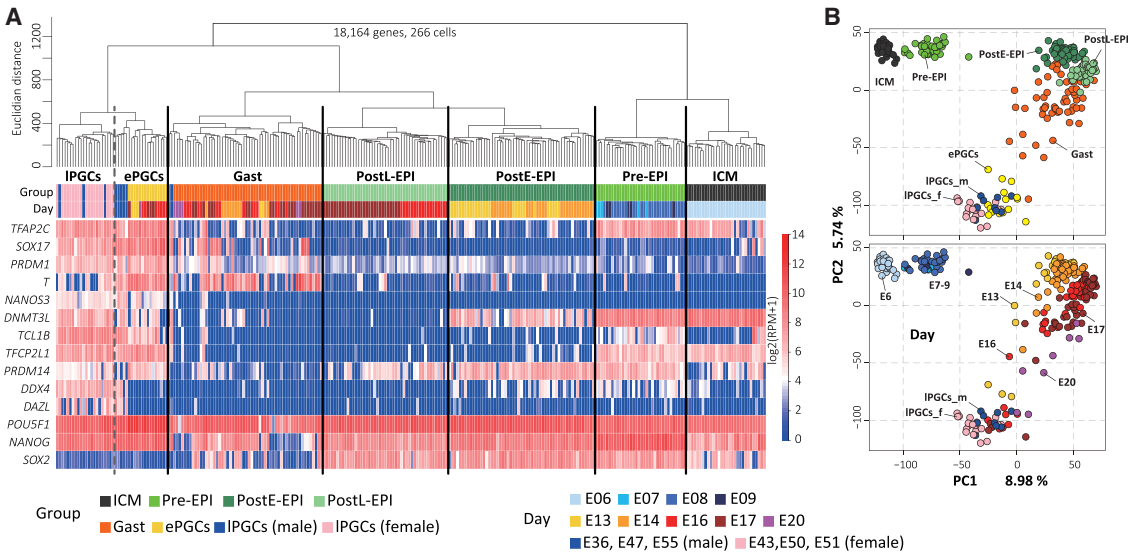

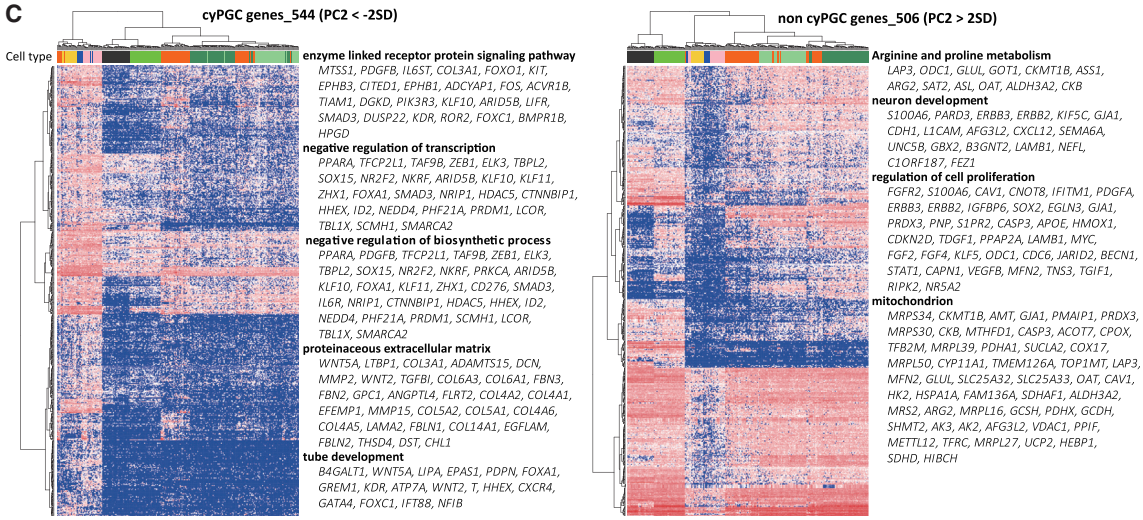

Figure 5. The Transcriptome of cyPGCs

(A) UHC with all expressed genes (log_2[RPM + 1] > 4 in at least one sample among 266 cells, 18,164 genes) and a heatmap of the levels of selected marker genes. Color bars under the dendrogram indicate cell types (top) and embryonic days (bottom), respectively. ICM, inner cell mass; pre-EPI, pre-implantation epiblast; postE-EPI, post-implantation early EPI; postL-EPI, post-implantation late EPI; Gast, gastrulating cells; ePGC, early PGC; lPGC, late PGC. The color coding is as indicated.

(B) PCA of all cells by all expressed genes as in (A). The cells (color coded as in A: upper, cell types; bottom, embryonic days) are plotted in a two-dimensional space defined by PC1 and 2.

(C) Heatmap of the expression of genes defined as highly contributing to the PC2 axis (cyPGC genes [left]: PC2 < −2SD; non-cyPGC genes [right]: PC2 > 2SD). The genes and cells were ordered by UHC. Color bars under the dendrogram indicate cell types (color coded as in A). Representative genes and key GO enrichments for each cluster are shown.

See also Figures S6 and S7.

et al., 2015; Sasaki et al., 2015), which would reflect a species-specific difference between humans and cynomolgus monkeys. We also noted that PDPN serves as a robust surface marker for cyPGCs and hPGCLCs (Figures 6C and 6D).

We identified differentially expressed genes (DEGs) between early and late cyPGCs (early PGC [the right cluster of ePGC in the dendrogram of Figure 5A] versus late PGC [the lPGC cluster]) (Figure 6E and Table S3). The early cyPGC genes (n = 48) included genes such as *T*, *GDF3*, and, consistent with the ISH analyses (Figure 4), targets of BMP4 signaling such as *ID1*, *ID2*, *MSX2*, and *SMAD7*, whereas the late cyPGC genes (n = 76) included *DDX4*, *DAZL*, *RNF1*, *DPEP2*, and *SPATA22*, and were enriched with GO terms for "gamete generation/sexual reproduction." Both UHCs using the early and late cyPGC genes clustered hPGCLCs closely with early cyPGCs (note that one early cyPGC was intermingled with hPGCLCs in the UHC using the early cyPGC genes) (Figure 6F). Thus, hPGCLCs in vitro bear a property similar to that of early cyPGCs just after their specification.

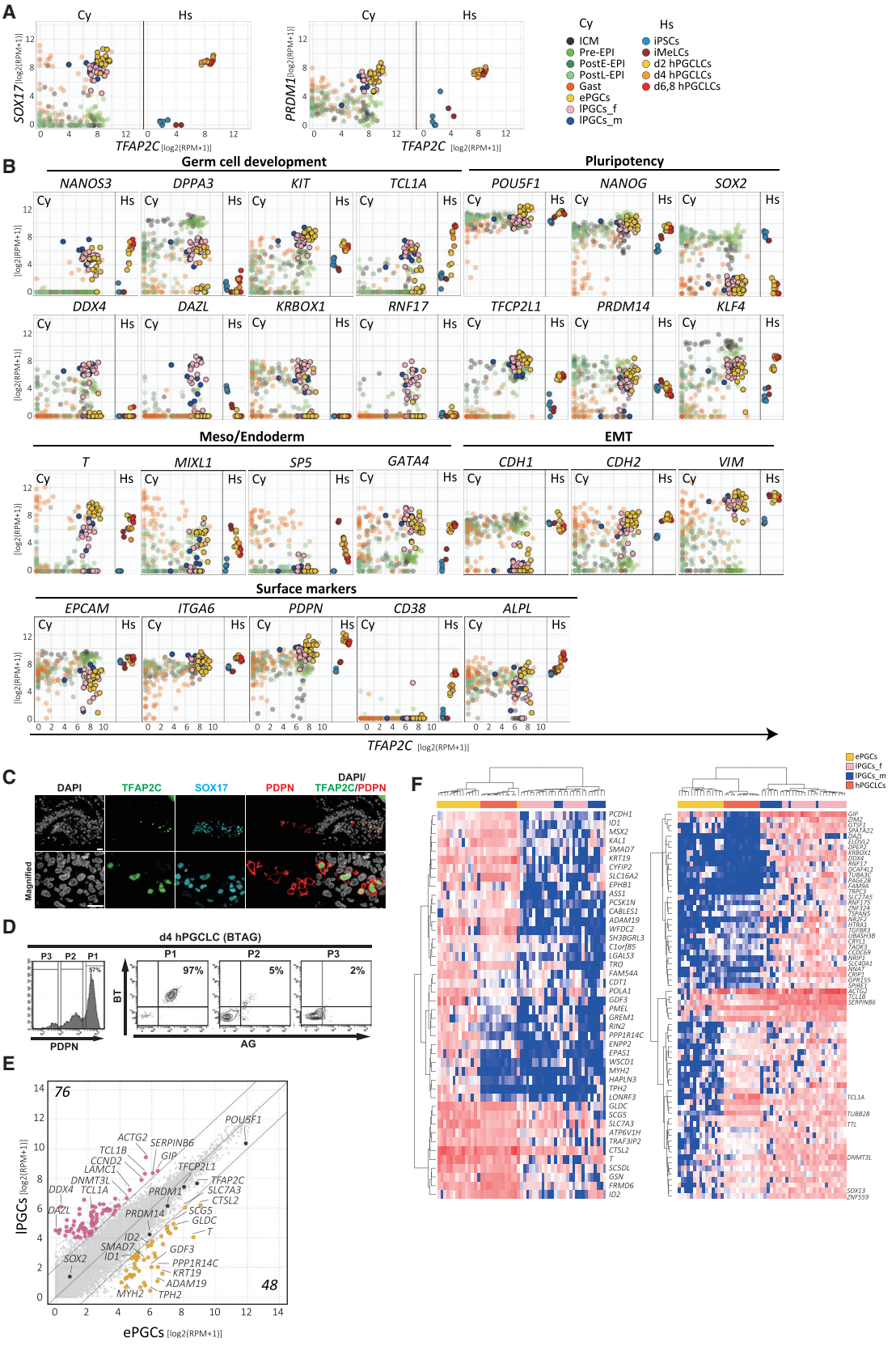

(legend on next page)

DISCUSSION

We have provided evidence for the notion that cyPGCs originate from the amnion (Figure 7): (1) the SOX17/TFAP2C/BLIMP1$^+$ cells are identified in the dorsal amnion as early as E11 prior to the onset of gastrulation (Figure 2); (2) such cells are positive for OCT4/NANOG/T and negative for SOX2/EOMES, a property consistent with hPGCLCs in vitro (Figures 3 and S5); (3) the amnion itself expresses *BMP4* and *WNT3A* (*WNT3A* is also expressed robustly in the cytotrophoblast), cytokines potentially critical for PGC specification, and the amnion responds primarily to them (Figure 4); and (4) cyPGCs as early as E13 show a transcriptome highly distinct from that of the epiblast (Figure 5). The cells consistent with the properties for cyPGCs continue to be detected at the posterior amnion at least by E17, and the posterior amnion continues to be a source for BMP4 as well (Figures 2, 4, and S5).

On the other hand, we cannot totally exclude the possibility that the posterior epiblast cells are recruited toward the amnion or between the epiblast and VE to differentiate into cyPGCs, particularly after E12/E13. This possibility is not necessarily mutually exclusive to the notion that cyPGCs originate primarily from the amnion, and some cyPGCs also arise from the epiblast. However, we did not detect SOX17$^+$ or TFAP2C$^+$ cells, or OCT4/NANOG/T$^+$ and SOX2/EOMES$^-$ cells, a potential precursor state of cyPGCs, within the posterior epiblast (Figures 2, 3, and S5). We also did not obtain evidence for cyPGC delamination from the epiblast (Figures 2, 3, and S5). These observations, together with the four lines of evidence that we describe above, have led us to consider this alternative possibility less plausible. Therefore, although the definitive conclusion awaits lineage tracing or real-time imaging, we propose that the amnion is the origin of the cy germ cell lineage. Considering the similarity in morphology/cell-fate allocations between cynomolgus monkey and human embryos, it is most likely that hPGCs also arise in the amnion.

Our finding is unexpected, since, based on the studies in mice, it has generally been assumed that the germ cell fate in mammals is specified in the epiblast along with gastrulation (Saitou and Yamaji, 2012). In mice, after implantation the epiblast continues to be in direct contact with the extra-embryonic ectoderm for a relatively longer period, and *Blimp1*$^+$ PGC precursors emerge in the most proximal posterior epiblast (Ohinata et al., 2005): thereafter, the amnion is specified along with gastrulation. In contrast, in primates the amnion is the first cell type that is segregated from the epiblast upon implantation, and the amnion directly contacts the cytotrophoblast until the extra-embryonic mesenchyme, which presumably arises from the VE (Enders and King, 1988; Luckett, 1978; Nakamura et al., 2016), intervenes between the amnion and the cytotrophoblast: SOX17/TFAP2C/BLIMP1$^+$ cyPGCs are first specified in the dorsal amnion, which is in direct contact with/in close proximity to the cytotrophoblast. Thus, the difference in the origin of PGCs between primates and mice (Figure 7) would be a reflection of the different strategies for cell-fate allocations and embryonic patterning between these species.

With regard to the mechanism of PGC specification, it is essential to take into consideration the inductive signals, their sources, and the competence of the cells responding to the signals (Saitou and Yamaji, 2012). Regarding the signals, in mice BMP4 from the extra-embryonic ectoderm and WNT3 from the proximal posterior epiblast are essential for conferring the germ cell fate onto the most proximal posterior epiblast (Figure 7) (Lawson et al., 1999; Ohinata et al., 2009). In cynomolgus monkeys, the present study, as well as studies on in vitro models in humans (Irie et al., 2015; Sasaki et al., 2015), suggests that BMP4 from the amnion and WNT3A both from the cytotrophoblast and the amnion would be critical for PGC specification. BMP4/2 from the extra-embryonic mesenchyme might also play a role. Thus, the key signals are likely to be very similar/homologous, but their sources and possibly their orders of action have diverged between mice and primates due to their structural divergence. The mechanism that specifically activates *BMP4* in the amnion warrants further investigation.

With regard to germ cell competence, in mice essentially all pre-gastrulating epiblast cells from E5.5 to E6.25 continue to bear such competence when provided with key signals (Ohinata et al., 2009). In cynomolgus monkeys, all the epiblast and amnion cells at PreG1 at E11, which are still morphologically relatively homogeneous and express OCT4/NANOG/SOX2 (Figures S3 and S5), most likely bear the competence for the germ cell fate, with the source of the inductive signals dictating the origin of PGCs: the dorsal amnion at E11 and the posterior amnion at least until E17. Accordingly, as part of the impact of inductive signals, the amnion represses SOX2 and acquires a distinct morphology prior to—and upregulates T coincident with—the

Figure 6. Early cyPGCs Are Similar to hPGCLCs

(A and B) Scatterplot comparison of the expressions of SOX17 and PRDM1 (A) or the indicated key genes (B) with that of TFAP2C in key cell types in cy embryos (left) and cells during hPGCLC induction (Sasaki et al., 2015) (right). iPSCs, induced pluripotent stem cells; iMeLC, incipient mesoderm-like cells; d, day; PGCLCs, PGC-like cells. The color coding is as indicated.

(C) IF images of the paraffin sections of cy embryos at E16 for TFAP2C (green), SOX17 (cyan), and PDPN (red) with a merge with DAPI (white). The magnified images are shown at the bottom. Scale bars, 20 μm.

(D) (Left) PDPN expression of day-4 aggregates induced from BLIMP1-2A-tdTomato and TFAP2C-2A-EGFP (BTAG) hiPSCs through iMeLCs (Sasaki et al., 2015), as assessed by FACS. (Right) BTAG expression in the three populations on the left gated according to the PDPN expression.

(E) Scatterplot comparison of the averaged gene expression levels between ePGCs (14 cells: the cells in the ePGC cluster of the dendrogram in Figure 5A without the lPGCm_d36 cluster) and lPGCs (22 cells: the cells in the lPGC cluster of the dendrogram in Figure 5A). Yellow, genes higher in ePGC; pink, genes higher in lPGC (more than 4-fold difference [flanking diagonal lines], mean $\log_2$[RPM + 1] > 4, FDR < 0.01). Key genes are annotated and the numbers of DEGs are indicated.

(F) Heatmap of the expression of DEGs defined in (E) in cyPGCs and hPGCLCs. The genes in common between humans and cynomolgus monkeys were used (high in ePGC: 44/48 genes [left]; high in lPGC: 70/76 genes [right]). The genes and samples were ordered by UHC. Color bars under the dendrogram indicate cell types.

See also Figures S6 and S7.

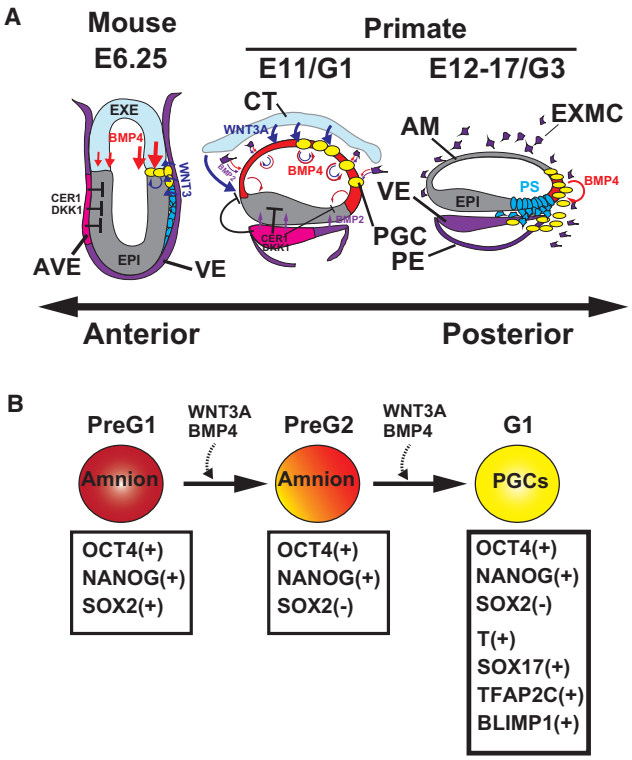

Figure 7. A Model for cyPGC Specification

(A) Schematic representation of a model for cyPGC specification at E11 (middle) and from E12 to E17 (right) in comparison with a model for mPGC specification at E6.25 (left). (Left) At E6.25, the proximal EPI receives BMP4 secreted from EXE and WNT3 from VE and EPI itself, which, together with inhibitory signals CER1 and DKK1 secreted from the anterior VE (AVE), specifies the PGCs at the most proximal posterior EPI. (Middle) At E11/G1, AM receives BMP4 secreted either from the AM itself or EXMC (also BMP2 from EXMC) and WNT3A secreted either from the trophectoderm or AM itself to be specified as cyPGCs (yellow). CER1 (BMP4 inhibitor) and DKK1 (WNT inhibitor) secreted from VE inhibit EPI to be specified as cyPGCs. (Right) From E12 to E17/G3, the posterior AM continues to receive BMP4 expressed by AM itself to be specified as cyPGCs. EXE, extra-embryonic ectoderm; AVE, anterior visceral endoderm; CT, cytotrophoblast; AM, amnion; EPI, epiblast; VE, visceral endoderm; PE, parietal endoderm; EXMC, extra-embryonic mesenchyme.

(B) TF expression during cyPGC specification.

upregulation of SOX17/TFAP2C/BLIMP1 (Figure 3). The upregulation of T, a key "mesodermal" factor, most likely in response to WNT3A signaling (Aramaki et al., 2013), prior to the onset of gastrulation suggests a unique morphogenetic event associated with the amnion development and cyPGC specification. Whether the epiblast cells bear the germ cell competence until a relatively late stage, e.g., E17, when provided with key signals is a critical question that warrants investigation.

We have recently shown that cy and hPSCs bear gene expression properties similar to those of post-implantation late epiblast (postL-EPI: E16, E17) and, to a lesser extent, post-implantation early epiblast (postE-EPI: E13, E14) cells (Nakamura et al., 2016). While we have shown here that cyPGCs are specified in the dorsal amnion as early as E11, cyPGC specification appeared to continue at least until E17 at the posterior amnion (Figures 2 and S5). As discussed earlier, the early dorsal amnion at E11 and posterior amnion until E17 were positive for OCT4 and NANOG (Figure S5), and as precursors for cyPGCs may continue to exhibit similar properties, which in turn may be similar to a state that the competent epiblast would acquire when exposed to signals such as the BMP4 and WNT signals. This might explain the competence of hPSCs for induction into the germ cell fate through a state similar to that in the incipient mesoderm (Irie et al., 2015; Sasaki et al., 2015). Additional comparisons between cyPGC and hPGC(LC) specification, including the single-cell RNA-seq analyses of the amnion at E11 and E12, although technically challenging, would be warranted. More precise dissection of the roles played by signaling molecules during hPGCLC induction would also be critical. Such studies as well as genetic studies exploring the roles of key TFs will reveal a more precise hierarchy of events leading to PGC specification in primates.

In conclusion, our study has clarified the origin and comprehensive development of PGCs in cynomolgus monkeys. Given the diversity inherent in the early development of mammals (Rossant, 2015), the mechanisms of PGC specification in extant mammals may also involve divergence, and warrant further investigation.

EXPERIMENTAL PROCEDURES

All of the animal experiments were performed under the ethical guidelines of Kyoto University and Shiga University of Medical Science. The procedures for staging of the embryo based on the localization of PGCs, IF analysis for 5mC on frozen sections and whole-mount IF analysis, ISH, transmission electron microscopy, FACS analysis of hPGCLCs, and determination of the sex of embryos are available in Supplemental Experimental Procedures.

Animals and Isolation of Post-implantation cy Embryos

Procedures using cynomolgus monkeys were approved by the Animal Care and Use Committee of the Shiga University of Medical Science. The series of reproductive technologies using cynomolgus monkeys, including oocyte collection, intra-cytoplasmic sperm injection, pre-implantation embryo culture, and transfer of pre-implantation embryos into foster mothers, were reported previously (Nakamura et al., 2016; Sasaki et al., 2015; Yamasaki et al., 2011). For the isolation of early post-implantation embryos, we transferred up to five embryos per foster mother.

Implanted embryos were scanned by transabdominal ultrasound monitoring and recovered either by cesarean section (later than E36 [embryos: n = 8]) or hysterectomy (E11–E28 [embryos: n = 50]), both under full anesthesia. The foster mothers were maintained after surgery. Genital ridges from embryos later than E36 were recovered as described previously (Sasaki et al., 2015). Embryos between E11 and E28 were recovered from the uterus according to the methods described previously (Nakamura et al., 2016; Yamasaki et al., 2011). In brief, the endometrium was exposed by dissection of the serosa and myometrium at the left lateral side of the explanted uterus, followed by careful dissection of the exposed endometrium along a cervix-to-fundus direction to approach the endometrial surfaces. Implantation sites, where trophoblastic reactions with ring-like congestion surrounding the central lucent region were typically present, were searched under dissection microscopy and photographed. The portion of the endometrium containing the embryo was blocked out and, whenever possible, chorionic membranes were removed for the correct orientation of the embryos for further analyses. We included the samples obtained by previous studies (Nakamura et al., 2016; Sasaki et al., 2015) for analysis.

Immunofluorescence Analysis on Paraffin Sections

For the IF analyses of embryos or embryonic gonads, the samples were fixed in 10% neutral formalin (Nakalai Tesque) overnight at room temperature. The samples were then embedded in paraffin, while maintaining the anterior-posterior (AP) orientation whenever possible. The samples were serially sectioned

at a thickness of 4 μm on a microtome and mounted on glass slides (Platinum Pro, Matsunami). The AP orientation was difficult to establish on many of the embryos at E11 and E12 under a dissection microscope due to their small size and/or the absence of an AP axis.

The paraffin sections were then de-paraffinized by xylene followed by rehydration. Slides were pretreated with HistVT One (Nakalai Tesque) for 35 min at 90°C, then for 15 min at room temperature for antigen retrieval. After washing three times with PBS, the slides were treated with blocking solution (5% normal donkey or goat serum, 0.2% Tween 20, 1× PBS) for 1 hr at room temperature before incubating with primary antibodies in blocking solution overnight at 4°C. The slides were then washed six times with PBS followed by incubation with secondary antibodies in blocking solution and 1 μg/mL DAPI for 50 min. Finally, the slides were washed six times with PBS before being mounted in Vectashield mounting medium (Vector Laboratories) for confocal laser scanning microscope analysis (Olympus FV1000 or Zeiss LSM 780).

The antibodies used in this study are listed in Supplemental Experimental Procedures.

Single-Cell cDNA Preparation and Transcriptome Analysis by Single-Cell mRNA 3′-End Sequencing

Single-cell cDNAs were prepared from early post-implantation cy embryos essentially as described previously (Kurimoto et al., 2006; Nakamura et al., 2015, 2016). For isolation of a relatively small population of cyPGCs, whole embryonic fragments containing epiblast (EPI), amnion, or secondary yolk sac (E13, one embryo; E14, two embryos; E16, one embryo; E17, one embryo), the posterior one-third (E16, one embryo), or fragments around the body stalk (E17, one embryo; E20, one embryo) were dissected out, and the tissue clumps were dissociated into single cells by incubating with 0.25% trypsin/PBS (T4799; Sigma-Aldrich) for around 10 min at 37°C followed by repeated pipetting. For the isolation of gonadal cyPGCs, genital ridges of E36, E47, E50, and E55 male embryos and E43, E50, and E51 female embryos (Sasaki et al., 2015) were dissected out and were dissociated into single cells by incubation with 0.25% trypsin/PBS for around 10 min at 37°C followed by repeated pipetting. The resulting single cells were dispersed in 0.1 mg/mL polyvinyl alcohol/PBS (P8136; Sigma-Aldrich) and were processed for the SC3-seq analysis.

The primers used in this study are listed in Supplemental Experimental Procedures.

Mapping Reads of SC3-Seq and Data Analysis

The genome sequence (GRCh37/hg19 for humans and MacFas5.0 for cynomolgus monkeys [*M. fascicularis*]) and the transcript annotation (ref_GRCh37 for humans and ref_MacFas5.0 for cynomolgus monkeys) were obtained from the NCBI ftp site at ftp://ftp-trace.ncbi.nlm.nih.gov/genomes/Macaca_fascicularis. The SC3-seq reads only the very 3′ end of transcripts, so that the expression levels were calculated as genes (Entrez genes) but not mRNAs. Read trimming, mapping, and estimation of expression levels were performed as described previously (Nakamura et al., 2016; Sasaki et al., 2015).

Data analysis was performed using R software version 3.1.1 with the gplots (ver. 2.16.0), qvalue (ver. 1.40.0), and genefilter (ver. 1.48.1) packages, and EXCEL (Microsoft), as described previously (Nakamura et al., 2016). All analyses of expression data were performed using $\log_2$(RPM + 1) values, where RPM is reads per million. We defined "all expressed genes" as genes whose $\log_2$(RPM + 1) values were >4 (>approximately 20 copies/cell) in at least one sample. UHC was performed using the hclust function with Euclidian distances and Ward distance functions (ward.D2). PCA was performed using the prcomp function without scaling. For identification of DEGs among multi-groups, the kruskal.test function for the Kruskal-Wallis test and the qvalue function were used to calculate the p value and false discovery rate (FDR), respectively. The DEGs were defined as the genes exhibiting more than 4-fold changes between the samples (FDR < 0.01), and the mean of the expression level of the group was >$\log_2$(RPM + 1) = 4. For the GO analysis using the DAVID web tool (Huang da et al., 2009), since the annotation of *M. fascicularis* genes was relatively incomplete, human annotation corresponding to that of cynomolgus monkeys was used. For this purpose, a one-to-one correspondence table of genes was made by genomic coordinate comparison using the LiftOver tool, as described previously (Nakamura et al., 2016; Sasaki et al., 2015).

ACCESSION NUMBERS

Accession numbers for the data generated in this study and for the published data used in this study are as follows: SC3-seq data (GEO: GSE76267), data for cells in the cyEPI lineage (GEO: GSE74767) (Nakamura et al., 2016), and the RNA-seq data of hPGCLCs (GEO: GSE67259) (Sasaki et al., 2015).

SUPPLEMENTAL INFORMATION

Supplemental Information includes Supplemental Experimental Procedures, seven figures, and three tables and can be found with this article online at http://dx.doi.org/10.1016/j.devcel.2016.09.007.

AUTHOR CONTRIBUTIONS

K.S. conducted the histology and the IF and ISH experiments and analyzed the data. T.N. and I.O. performed the SC3-seq experiments, and T.N. analyzed the SC3-seq data. Y.Y. and T.Y. contributed to the SC3-seq data. C.I., H.T., Y.S., and S.N. contributed to the isolation of cynomolgus embryos. N.S. and T.T. contributed to the 3D reconstruction of the histological sections. K.S. and M.S. conceived the project, designed the experiments, and wrote the manuscript.

ACKNOWLEDGMENTS

We are grateful to the Center for Anatomical, Pathological and Forensic Medical Research at Kyoto University for the preparation of paraffin sections and electron microscopy, and to the animal care staff at the Research Center for Animal Life Science, Shiga University of Medical Science for assistance. We thank the members of our laboratory for their discussion of this study; Y. Nagai, R. Kabata, N. Konishi, Y. Sakaguchi, and M. Kawasaki of the Saitou Laboratory, and T. Sato and M. Kabata of the Yamamoto Laboratory for their technical assistance; and M. Ema for encouragement. K.S. thanks T.Q. Nguyen for the translation of the relevant literature written in German into English. This work was supported in part by a Grant-in-Aid from MEXT and by JST-ERATO.

Received: April 2, 2016
Revised: July 23, 2016
Accepted: September 12, 2016
Published: October 6, 2016

REFERENCES

Aramaki, S., Hayashi, K., Kurimoto, K., Ohta, H., Yabuta, Y., Iwanari, H., Mochizuki, Y., Hamakubo, T., Kato, Y., Shirahige, K., et al. (2013). A mesodermal factor, T, specifies mouse germ cell fate by directly activating germline determinants. Dev. Cell *27*, 516–529.

Arnold, S.J., and Robertson, E.J. (2009). Making a commitment: cell lineage allocation and axis patterning in the early mouse embryo. Nat. Rev. Mol. Cell Biol. *10*, 91–103.

Buaas, F.W., Kirsh, A.L., Sharma, M., McLean, D.J., Morris, J.L., Griswold, M.D., de Rooij, D.G., and Braun, R.E. (2004). Plzf is required in adult male germ cells for stem cell self-renewal. Nat. Genet. *36*, 647–652.

Costoya, J.A., Hobbs, R.M., Barna, M., Cattoretti, G., Manova, K., Sukhwani, M., Orwig, K.E., Wolgemuth, D.J., and Pandolfi, P.P. (2004). Essential role of Plzf in maintenance of spermatogonial stem cells. Nat. Genet. *36*, 653–659.

de Jong, J., Stoop, H., Gillis, A.J., van Gurp, R.J., van de Geijn, G.J., Boer, M., Hersmus, R., Saunders, P.T., Anderson, R.A., Oosterhuis, J.W., et al. (2008). Differential expression of SOX17 and SOX2 in germ cells and stem cells has biological and clinical implications. J. Pathol. *215*, 21–30.

Eckert, D., Biermann, K., Nettersheim, D., Gillis, A.J., Steger, K., Jack, H.M., Muller, A.M., Looijenga, L.H., and Schorle, H. (2008). Expression of BLIMP1/PRMT5 and concurrent histone H2A/H4 arginine 3 dimethylation in fetal germ cells, CIS/IGCNU and germ cell tumors. BMC Dev. Biol. *8*, 106.

Enders, A.C. (2007). Implantation in the macaque: expansion of the implantation site during the first week of implantation. Placenta *28*, 794–802.

Enders, A.C., and King, B.F. (1988). Formation and differentiation of extraembryonic mesoderm in the rhesus monkey. Am. J. Anat. *181*, 327–340.

Enders, A.C., Schlafke, S., and Hendrickx, A.G. (1986). Differentiation of the embryonic disc, amnion, and yolk sac in the rhesus monkey. Am. J. Anat. *177*, 161–185.

Extavour, C.G., and Akam, M. (2003). Mechanisms of germ cell specification across the metazoans: epigenesis and preformation. Development *130*, 5869–5884.

Gerdes, J., Lemke, H., Baisch, H., Wacker, H.H., Schwab, U., and Stein, H. (1984). Cell cycle analysis of a cell proliferation-associated human nuclear antigen defined by the monoclonal antibody Ki-67. J. Immunol. *133*, 1710–1715.

Ginsburg, M., Snow, M.H., and McLaren, A. (1990). Primordial germ cells in the mouse embryo during gastrulation. Development *110*, 521–528.

Gkountela, S., Zhang, K.X., Shafiq, T.A., Liao, W.W., Hargan-Calvopina, J., Chen, P.Y., and Clark, A.T. (2015). DNA demethylation dynamics in the human prenatal germline. Cell *161*, 1425–1436.

Guo, F., Yan, L., Guo, H., Li, L., Hu, B., Zhao, Y., Yong, J., Hu, Y., Wang, X., Wei, Y., et al. (2015). The transcriptome and DNA methylome landscapes of human primordial germ cells. Cell *161*, 1437–1452.

Hamada, F., Tomoyasu, Y., Takatsu, Y., Nakamura, M., Nagai, S., Suzuki, A., Fujita, F., Shibuya, H., Toyoshima, K., Ueno, N., et al. (1999). Negative regulation of Wingless signaling by D-axin, a *Drosophila* homolog of axin. Science *283*, 1739–1742.

Hayashi, K., Ohta, H., Kurimoto, K., Aramaki, S., and Saitou, M. (2011). Reconstitution of the mouse germ cell specification pathway in culture by pluripotent stem cells. Cell *146*, 519–532.

Heuser, C.H., and Streeter, G.L. (1941). Development of the macaque embryo. Contrib. Embryol. *29*, 41.

Hollnagel, A., Oehlmann, V., Heymer, J., Ruther, U., and Nordheim, A. (1999). Id genes are direct targets of bone morphogenetic protein induction in embryonic stem cells. J. Biol. Chem. *274*, 19838–19845.

Hoyer, P.E., Byskov, A.G., and Mollgard, K. (2005). Stem cell factor and c-Kit in human primordial germ cells and fetal ovaries. Mol. Cell Endocrinol. *234*, 1–10.

Hu, Y.C., Okumura, L.M., and Page, D.C. (2013). Gata4 is required for formation of the genital ridge in mice. PLoS Genet. *9*, e1003629.

Huang da, W., Sherman, B.T., and Lempicki, R.A. (2009). Systematic and integrative analysis of large gene lists using DAVID bioinformatics resources. Nat. Protoc. *4*, 44–57.

Irie, N., Weinberger, L., Tang, W.W., Kobayashi, T., Viukov, S., Manor, Y.S., Dietmann, S., Hanna, J.H., and Surani, M.A. (2015). SOX17 is a critical specifier of human primordial germ cell fate. Cell *160*, 253–268.

Kurimoto, K., Yabuta, Y., Ohinata, Y., Ono, Y., Uno, K.D., Yamada, R.G., Ueda, H.R., and Saitou, M. (2006). An improved single-cell cDNA amplification method for efficient high-density oligonucleotide microarray analysis. Nucleic Acids Res. *34*, e42.

Kurimoto, K., Yabuta, Y., Ohinata, Y., Shigeta, M., Yamanaka, K., and Saitou, M. (2008). Complex genome-wide transcription dynamics orchestrated by Blimp1 for the specification of the germ cell lineage in mice. Genes Dev. *22*, 1617–1635.

Kurimoto, K., Yabuta, Y., Hayashi, K., Ohta, H., Kiyonari, H., Mitani, T., Moritoki, Y., Kohri, K., Kimura, H., Yamamoto, T., et al. (2015). Quantitative dynamics of chromatin remodeling during germ cell specification from mouse embryonic stem cells. Cell Stem Cell *16*, 517–532.

Lawson, K.A., Dunn, N.R., Roelen, B.A., Zeinstra, L.M., Davis, A.M., Wright, C.V., Korving, J.P., and Hogan, B.L. (1999). Bmp4 is required for the generation of primordial germ cells in the mouse embryo. Genes Dev. *13*, 424–436.

Luckett, W.P. (1978). Origin and differentiation of the yolk sac and extraembryonic mesoderm in presomite human and rhesus monkey embryos. Am. J. Anat. *152*, 59–97.

Mamsen, L.S., Brochner, C.B., Byskov, A.G., and Mollgard, K. (2012). The migration and loss of human primordial germ stem cells from the hind gut epithelium towards the gonadal ridge. Int. J. Dev. Biol. *56*, 771–778.

McLaren, A. (2003). Primordial germ cells in the mouse. Dev. Biol. *262*, 1–15.

Nakamura, T., Yabuta, Y., Okamoto, I., Aramaki, S., Yokobayashi, S., Kurimoto, K., Sekiguchi, K., Nakagawa, M., Yamamoto, T., and Saitou, M. (2015). SC3-seq: a method for highly parallel and quantitative measurement of single-cell gene expression. Nucleic Acids Res. *43*, e60.

Nakamura, T., Okamoto, I., Sasaki, K., Yabuta, Y., Iwatani, C., Tsuchiya, H., Seita, Y., Nakamura, S., Yamamoto, T., and Saitou, M. (2016). A developmental coordinate of pluripotency among mice, monkeys and humans. Nature *537*, 57–62.

O'Rahilly, R., and Müller, F. (1987). Developmental Stages in Human Embryos Including a Revision of Streeter's 'Horizons' and a Survey of the Carnegie Collection (Carnegie Institution), p. 637.

Ohinata, Y., Payer, B., O'Carroll, D., Ancelin, K., Ono, Y., Sano, M., Barton, S.C., Obukhanych, T., Nussenzweig, M., Tarakhovsky, A., et al. (2005). Blimp1 is a critical determinant of the germ cell lineage in mice. Nature *436*, 207–213.

Ohinata, Y., Ohta, H., Shigeta, M., Yamanaka, K., Wakayama, T., and Saitou, M. (2009). A signaling principle for the specification of the germ cell lineage in mice. Cell *137*, 571–584.

Pauls, K., Jager, R., Weber, S., Wardelmann, E., Koch, A., Buttner, R., and Schorle, H. (2005). Transcription factor AP-2gamma, a novel marker of gonocytes and seminomatous germ cell tumors. Int. J. Cancer *115*, 470–477.

Perrett, R.M., Turnpenny, L., Eckert, J.J., O'Shea, M., Sonne, S.B., Cameron, I.T., Wilson, D.I., Rajpert-De Meyts, E., and Hanley, N.A. (2008). The early human germ cell lineage does not express SOX2 during in vivo development or upon in vitro culture. Biol. Reprod. *78*, 852–858.

Politzer, G. (1930). Uber einen menschlichen Embryo mit 7 Urwirbelpaaren. 3. Das Entoderm. Z. Anat. Entw. Gesch *93*, 386–428.

Politzer, G. (1933). Die Keimbahn des Menschen. Z. Anat. Entw. Gesch *100*, 331–336.

Rossant, J. (2015). Mouse and human blastocyst-derived stem cells: vive les differences. Development *142*, 9–12.

Russ, A.P., Wattler, S., Colledge, W.H., Aparicio, S.A., Carlton, M.B., Pearce, J.J., Barton, S.C., Surani, M.A., Ryan, K., Nehls, M.C., et al. (2000). Eomesodermin is required for mouse trophoblast development and mesoderm formation. Nature *404*, 95–99.

Saitou, M., and Miyauchi, H. (2016). Gametogenesis from pluripotent stem cells. Cell Stem Cell *18*, 721–735.

Saitou, M., and Yamaji, M. (2012). Primordial germ cells in mice. Cold Spring Harb. Perspect. Biol. *4*, http://dx.doi.org/10.1101/cshperspect.a008375.

Saitou, M., Barton, S.C., and Surani, M.A. (2002). A molecular programme for the specification of germ cell fate in mice. Nature *418*, 293–300.

Sasaki, K., Yokobayashi, S., Nakamura, T., Okamoto, I., Yabuta, Y., Kurimoto, K., Ohta, H., Moritoki, Y., Iwatani, C., Tsuchiya, H., et al. (2015). Robust in vitro induction of human germ cell fate from pluripotent stem cells. Cell Stem Cell *17*, 178–194.

Seguin, C.A., Draper, J.S., Nagy, A., and Rossant, J. (2008). Establishment of endoderm progenitors by SOX transcription factor expression in human embryonic stem cells. Cell Stem Cell *3*, 182–195.

Seki, Y., Hayashi, K., Itoh, K., Mizugaki, M., Saitou, M., and Matsui, Y. (2005). Extensive and orderly reprogramming of genome-wide chromatin modifications associated with specification and early development of germ cells in mice. Dev. Biol. *278*, 440–458.

Soudais, C., Bielinska, M., Heikinheimo, M., MacArthur, C.A., Narita, N., Saffitz, J.E., Simon, M.C., Leiden, J.M., and Wilson, D.B. (1995). Targeted mutagenesis of the transcription factor GATA-4 gene in mouse embryonic stem cells disrupts visceral endoderm differentiation in vitro. Development *121*, 3877–3888.

Tang, W.W., Dietmann, S., Irie, N., Leitch, H.G., Floros, V.I., Bradshaw, C.R., Hackett, J.A., Chinnery, P.F., and Surani, M.A. (2015). A unique gene regulatory network resets the human germline epigenome for development. Cell *161*, 1453–1467.

Vincent, S.D., Dunn, N.R., Sciammas, R., Shapiro-Shalef, M., Davis, M.M., Calame, K., Bikoff, E.K., and Robertson, E.J. (2005). The zinc finger transcriptional repressor Blimp1/Prdm1 is dispensable for early axis formation but is required for specification of primordial germ cells in the mouse. Development *132*, 1315–1325.

Weber, S., Eckert, D., Nettersheim, D., Gillis, A.J., Schafer, S., Kuckenberg, P., Ehlermann, J., Werling, U., Biermann, K., Looijenga, L.H., et al. (2010). Critical function of AP-2 gamma/TCFAP2C in mouse embryonic germ cell maintenance. Biol. Reprod. *82*, 214–223.

Weismann, A. (1892). Das Keimplasma. Eine Theorie der Vererbung (Gustav Fischer).

Witschi, E. (1948). Migration of germ cells of human embryos from the yolk sac to the primitive gonadal folds. Contrib. Embryol. *209*, 67–80.

Yamaji, M., Seki, Y., Kurimoto, K., Yabuta, Y., Yuasa, M., Shigeta, M., Yamanaka, K., Ohinata, Y., and Saitou, M. (2008). Critical function of Prdm14 for the establishment of the germ cell lineage in mice. Nat. Genet. *40*, 1016–1022.

Yamaji, M., Ueda, J., Hayashi, K., Ohta, H., Yabuta, Y., Kurimoto, K., Nakato, R., Yamada, Y., Shirahige, K., and Saitou, M. (2013). PRDM14 ensures naive pluripotency through dual regulation of signaling and epigenetic pathways in mouse embryonic stem cells. Cell Stem Cell *12*, 368–382.

Yamasaki, J., Iwatani, C., Tsuchiya, H., Okahara, J., Sankai, T., and Torii, R. (2011). Vitrification and transfer of cynomolgus monkey (*Macaca fascicularis*) embryos fertilized by intracytoplasmic sperm injection. Theriogenology *76*, 33–38.